KLOE note # 174
April 2002

Measurement of $\Gamma(K_S \to \pi^+\pi^-)/\Gamma(K_S \to \pi^0\pi^0)$ with KLOE 2000 data.

M. Palutan,
Università di Roma "Tor Vergata" and INFN, Laboratori Nazionali di Frascati

T. Spadaro,
INFN, Laboratori Nazionali di Frascati

P. Valente
INFN, Laboratori Nazionali di Frascati

Abstract

A detailed description of the measurement of the ratio $\Gamma(K_S \to \pi^+\pi^-)/\Gamma(K_S \to \pi^0\pi^0)$ with the KLOE year 2000 data sample is given. The $K_S \to \pi^+\pi^-$ and $K_S \to \pi^0\pi^0$ decays are tagged by the identification of K_L interactions in the calorimeter. Details are given about the K_S-tagging procedure and efficiencies for the two decay modes; the selection algorithms are then described, and the efficiencies entering the ratio are evaluated. Finally, all the contributions to the systematic error are discussed.

Contents

1 Motivations and measurement method

The measurement of $\Gamma(K_S \to \pi^+\pi^-)/\Gamma(K_S \to \pi^0\pi^0)$ constitutes the K_S-part of the double ratio, used to estimate $\Re(\varepsilon'/\varepsilon)$. Hence, the goal for the relative accuracy amounts to few 10^{-3}.

In KLOE K_S decays are tagged efficiently by the identification of a K_L interaction in the calorimeter, the so called "K_L crash"; this idea can be actually be exploited thanks to the exceptional timing performance of the calorimeter and to the fact that the K_L velocity is as low as $0.2c$. The typical $K_{\rm crash}$ event is shown in Fig. 1.

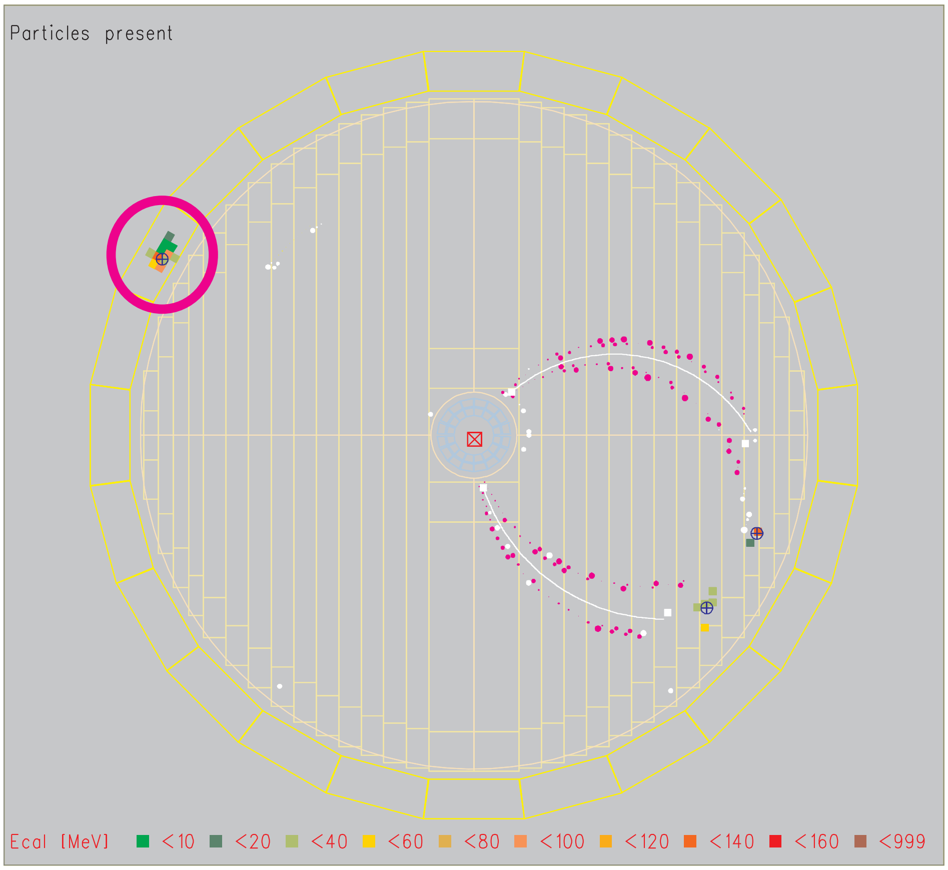

Figure 1: A typical K_S selected event: the K_S is tagged identifying a $K_{\rm crash}$ cluster in the calorimeter.

Even if this tag maximizes the spatial separation of the kaons, this condition does not necessarily imply that the K_S tagging efficiency is independent of the K_S decay mode. Therefore the tag bias, which depends ultimately on the method used to fix the "time zero" of the event, has been therefore carefully considered.

Simple criteria have been applied to K_S-tagged events: three or more calorimeter clusters with a timing compatible with the hypothesis of prompt photons, to select $K_S \to \pi^0\pi^0$ events; two oppositely charged tracks originating from the IP, to select $K_S \to \pi^+\pi^-$ events. Already with this loose selection cuts, the background level coming from channels other than $K_S \to \pi^+\pi^-$ and $K_S \to \pi^0\pi^0$ is kept well below 1%.

Summarizing, in order to be identified, a $K_S \to \pi^+\pi^-(\pi^0\pi^0)$ event has to be triggered, to satisfy the $K_{\rm crash}$-tagging cuts (a golden-t_0 cluster and a $K_{\rm crash}$-cluster have to be found), and the ones of a selection algorithm. Hence, the global efficiency $\varepsilon_{\rm tot}^{\pm(00)}$ of these requirements has to be estimated in order to obtain from the number of observed events $N^{\pm}$ (N^{00}), the $T^{\pm}$ (T^{00}) truly produced events:

$$N^{\pm(00)} = \underbrace{\mathcal{L}\sigma_{\phi}\mathrm{BR}(\phi \to \mathrm{K_S K_L})\mathrm{BR}[\mathrm{K_S} \to \pi^+\pi^-(\pi^0\pi^0)]}_{T^{\pm(00)}} \times \varepsilon_{\mathrm{tot}}^{\pm(00)}$$

The integrated luminosity $\mathcal{L}$ and the cross section of production $\sigma_{\phi}\mathrm{BR}(\phi \to \mathrm{K_S K_L})$ exactly cancel out in the calculation of the ratio of the number of events observed in the two K_S channels, allowing the measurement of the ratio of branching fractions:

$$\frac{N^{\pm}}{N^{00}} = \frac{\mathrm{BR}(\mathrm{K_S} \to \pi^+\pi^-)}{\mathrm{BR}(\mathrm{K_S} \to \pi^0\pi^0)} \times \frac{\varepsilon_{\mathrm{tot}}^{\pm}}{\varepsilon_{\mathrm{tot}}^{00}} \tag{1}$$

The total efficiencies are expressed as a product of efficiencies of the single requirements. These, in turn, have to be calculated as conditional probabilities, given the previously applied cuts. In order to simplify the efficiency estimates, the sequence of the cuts (all put in logical-AND) can be reordered. In the chosen scheme the total efficiencies are expressed as follows:

$$\varepsilon_{\mathrm{tot}}^{\pm(00)} = \varepsilon_{\mathrm{crash}}(E_{\mathrm{cut}}) \cdot \varepsilon_{\mathrm{sele}}^{\pm(00)} \cdot \varepsilon_{\mathrm{t0trg}}^{\pm(00)} \cdot \varepsilon_{\mathrm{tag}}^{\pm(00)} \cdot \varepsilon_{\mathrm{veto}}^{\pm(00)}$$

where:

- the efficiency $\varepsilon_{\mathrm{crash}}$ for the K_L to produce a K_{crash}-cluster with energy greater than E_{cut} is independent of the particular K_S decay mode and cancels out in the ratio of efficiencies Eq. (1);
- the efficiencies $\varepsilon_{\mathrm{sele}}^{00,\pm}$ of the selection algorithms described in Sect. 3 and 7, are calculated given the K_{crash}-tag, as discussed in Sect. 4 and 8;
- the t_0 and trigger efficiencies $\varepsilon_{\mathrm{t0trg}}^{00,\pm}$ are calculated for the selected events in Sect. 5 and 10;
- the ratio of tagging efficiency corrections $R_{\mathrm{tag}}^{\pm/00} = \varepsilon_{\mathrm{tag}}^{\pm}/\varepsilon_{\mathrm{tag}}^{00}$, specific of each K_S-channel due to the different t_0 estimate, is discussed in Sect. 2.3;
- the corrections due to the cosmic-veto are discussed in Sect. 11.

To reach the aimed level of precision all the relevant corrections such as clustering, tracking, trigger and tagging efficiencies have been estimated mainly using data subsamples, not to rely exclusively on the Monte Carlo simulation on such critical aspects of the measurement. The Monte Carlo has been instead used for the calculation of the geometrical acceptance, which represents anyway the dominant part of the overall selection efficiency.

Another relevant aspect in this measurement is the evaluation of the weight of the $K_S \to \pi^+\pi^-(\gamma)$, as a function of the energy of the emitted photon. It is important to establish the range of validity of the $K_S \to \pi^+\pi^-$ measurement, by specifying the effective cutoff on the photon energy implied by the analysis. Indeed, since at present no $K^0 \to \pi\pi$ branching ratio is known with well defined conditions on the radiated photon, the extraction of the isospin-definite amplitudes from the measured widths is affected by a larger uncertainty than that obtained just by propagating the experimental errors. This aspect makes the measurement interesting *per se*.

After having discussed in detail all the steps of the tagging and selection procedure (Sect. 2-11), the result for the ratio of decay widths based on 2000 dataset will be evaluated in Sect. 12, with short comments on the accuracy achieved on statistic and systematic error. Finally, in Sect. 13, conclusions and future perspectives are discussed. The final result is consistent with the one obtained with the analysis performed on the 1999 dataset (discussed in [1]), which served as a starting point for the present work.

1.1 Data sample

Data of the KLOE year 2000 running period have been used, after the official reconstruction [2, 3] had runned and classification algorithm had divided events in different "streams" [4]. The signal has been selected from the main K_S-tag sample represented by the *kcrash* stream [5]. Other data subsamples were extensively used for the various efficiency estimates, in particular events from the *kltag* [6] and *ksneut* [7] streams. Details about the event reconstruction and classification algorithms are given in the cited references.

Since the standard KLOE *ntuple*-production was used, the analyzed dataset represents the 70% of the year 2000 statistics (≈ 17 pb^{-1}). These data were then divided in four subsamples, as reported in Tab. 1, in order to check the stability of the detection and selection efficiencies.

Running period	Range of runs	Integrated luminosity
15/07 $\rightarrow$ 05/08	14075 $\rightarrow$ 14678	3.53 pb^{-1}
30/10 $\rightarrow$ 15/11	16211 $\rightarrow$ 16712	6.15 pb^{-1}
15/11 $\rightarrow$ 24/11	16713 $\rightarrow$ 17010	3.90 pb^{-1}
24/11 $\rightarrow$ 06/12	17011 $\rightarrow$ 17249	3.92 pb^{-1}
Total		17.34 pb^{-1}

Table 1: Year 2000 data samples used for the present analysis.

2 Tagging of the K_S

In KLOE roughly 50% of the produced K_L's reach the calorimeter before decaying. The fraction of K_L decays in a fiducial volume

$$30 \text{ cm} \leq \sqrt{x^2 + y^2} \leq 180 \text{ cm} \ ; \ |z| \leq 150 \text{ cm}$$

is roughly of 30%, while $\sim 12\%$ is the probability that the K_L decays before reaching the drift chamber volume:

$$\sqrt{x^2 + y^2} \leq 25 \text{ cm}$$

Moreover, total angular momentum conservation of the spin-1 ϕ meson determine the angular distribution of the produced kaons:

$$\frac{\mathrm{d}N}{\mathrm{d}\Omega} \propto \sin^2\theta,$$

where θ is the angle of the $K_{S,L}$ momentum in the ϕ rest frame with respect to the beam axis. The small ϕ boost only slightly affects the angular distribution; so the previous relation roughly applies to the laboratory, too. The probability that a K_L reaches the barrel calorimeter before decaying is so a factor of 1.18 higher than that to reach the end-cap.

The K_L is the slowest particle produced in the IP that can reach the calorimeter before decaying; charged kaons, in fact, lose a relevant fraction of their energy traversing the materials, have a mean decay length of ~ 90 cm, and reach the calorimeter with small probability. Since the emitted K_L's are almost monochromatic, the identification of the K_L interaction ("K_{crash}") in the calorimeter can be performed through a time-of-flight technique, described in Sect. 2.2. Since the value of cluster times is used for the velocity calculation, it is necessary to explicitly define an algorithm to fix the global event offset (t_0^G) as described in Sect. 2.1.

2.1 t_0 fixing

The absolute time scale is set by subtracting a common offset t_0^G from all the calorimeter cell (and cluster) measured times. As a first order approximation this "global-t_0" is fixed using the *fastest* cluster of the event, the so called t_0-cluster, assuming that this is due to a prompt photon coming from the interaction point (*T0STEP0* algorithm):

$$t_{t0}^{TOF} = \frac{\sqrt{x_{\rm CL}^2 + y_{\rm CL}^2 + z_{\rm CL}^2}}{c} = \frac{|\mathbf{r}_{\rm CL}|}{c} \tag{2}$$

The global-t_0 is then related to the fixed delay $\delta_{\rm cable}$ of the signals coming from the calorimeter TDC's, to the time of the t_0-fixing cluster $t_{\rm t0CL}$, and to its time-of-flight:

$$t_0^G = \delta_{\rm cable} - {\rm Nint}\left[\frac{t_{\rm t0}^{\rm TOF} - t_{\rm TOCL} + \delta_{\rm cable}}{T_{\rm bunch}}\right] \times T_{\rm bunch} \tag{3}$$

where "Nint" stands for the nearest integer and $T_{\rm bunch}$ is the nominal inter-bunch time spacing.

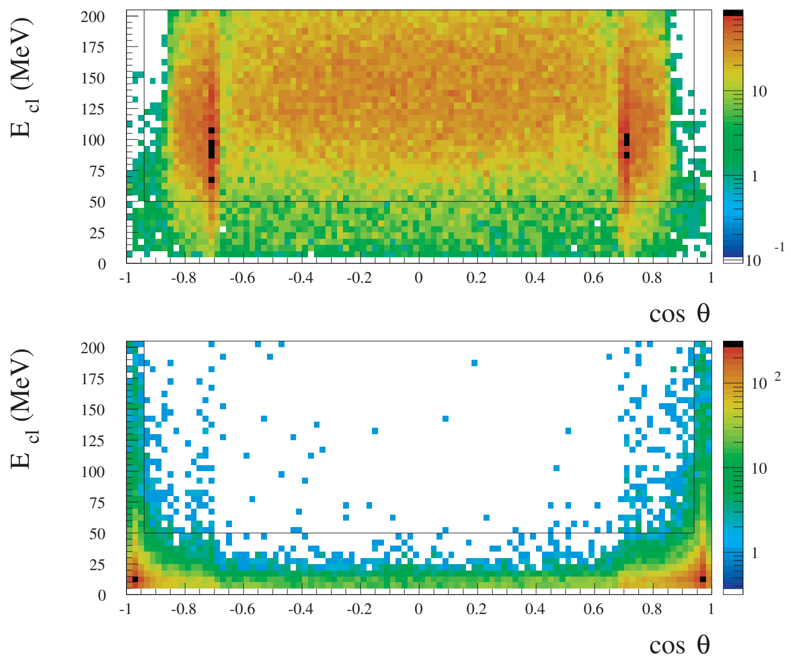

Figure 2: Energy of the cluster vs. polar angle for $K_S \to \pi^+\pi^-$ events (top) and accidental clusters (bottom). The cut imposed to reject low energy clusters entering the calorimeter at small θ angles is also shown.

In order to minimize the probability that the t_0-cluster is actually an accidental, a cut is imposed to reject the soft-energy, low-θ region, as shown in Fig. 2. The t_0-cluster is defined as the one having the lowest time among those satisfying:

$$E_{\rm CL} > 50 \text{ MeV} \ , \ \sqrt{x_{\rm CL}^2 + y_{\rm CL}^2} > 60 \text{ cm} \tag{4}$$

If no cluster satisfies this requirement, the event is rejected.

2.2 K_L cluster selection

The selection is performed after the full reconstruction of the event. For each "neutral" cluster (not associated to any track), with centroid-position with respect to the origin $\mathbf{r}_{\rm CL}$ and centroid-time $t_{\rm CL}$, the laboratory velocity is calculated:

$$\beta = \frac{|\mathbf{r}_{\rm CL}|}{c \cdot t_{\rm CL}}$$

The ϕ *nominal* velocity $\langle \beta_\phi \rangle = 0.0127$ and and the angle α between the position-vector $\mathbf{r}_{\rm CL}$ and the ϕ *nominal* momentum are used to calculate the velocity β^* of the cluster in the ϕ rest frame:

$$\beta^* = \frac{\sqrt{\langle \beta_\phi \rangle^2 + \beta^2 + 2 \langle \beta_\phi \rangle \beta \cos\alpha}}{1 + \langle \beta_\phi \rangle \beta \cos\alpha}$$

The distribution of β^* as a function of the cluster energy is shown in Fig. 3 for $K_S \to \pi^0\pi^0$ and $K_S \to \pi^+\pi^-$ events, selected with *kltag* and *ksneut* identification algorithms.

For cluster energies above 100 MeV the β^* variable peaks at two different values, depending on the K_S decay mode, as shown in Fig. 4.

This is due the global-t_0 estimate: in $K_S \to \pi^0\pi^0$ events the hypothesis of Eq. (2) is correct, since the fastest cluster is actually due to a K_S photon, with time-of-flight around $6-7$ ns; this is not true for $K_S \to \pi^+\pi^-$ events. In this case, the fastest pion-cluster has a time-of-flight of ~ 10 ns, since the pion velocity is ~ 0.8. So, the TOF is underestimated and the global-t_0 estimate exceeds the correct value.

In Fig. 5 the difference between the correct t_0 (calculated using the measured track lenght and the correct pion velocity) and the one calculated using the photon hyphotesis is shown: more than 90% of $K_S \to \pi^+\pi^-$ events have an error $-1 \cdot T_{\rm bunch}$.

In the present analysis all the neutral clusters satisfying:

$$E_{\rm CL} > 100 \text{ MeV}$$
$$0.195 \leq \beta^* \leq 0.2475$$

are called "$K_{\rm crash}$-clusters". The chosen cuts comprehend both peaks. The tuning of the β^* window and energy limits are discussed in the following.

The background to the tagging algorithm is not a problem for the final selection, since any residual contamination for both the charged and neutral signals is easily removed by the acceptance cuts on the K_S side, discussed in the following sections. Anyhow, the background has to be minimized in order to reduce the data volume occupied by the tagged events. The main contamination comes from cosmic rays surviving the background filter (*FILFO* [8]) entering the apparatus through the intersection between barrel and end-cap. For this reason, an acceptance cut has been imposed, selecting $K_{\rm crash}$-clusters in the barrel. The corresponding geometrical acceptance cancels out in the ratio measurement. Moreover, muons entering the calorimeter surface at an angle with respect to the normal direction (as in the example in Fig. 6), have long "paths" inside the calorimeter. It is then possible to reject them counting the maximum number $N_{\rm cc}$ of adjacent hit columns in the barrel, where a hit column is defined by an energy deposit above 7 MeV. Requiring $N_{\rm cc} \leq 5$ the final contamination is around 20%. The flow diagram of the $K_{\rm crash}$ selection algorithm is finally summarized in Fig. 7.

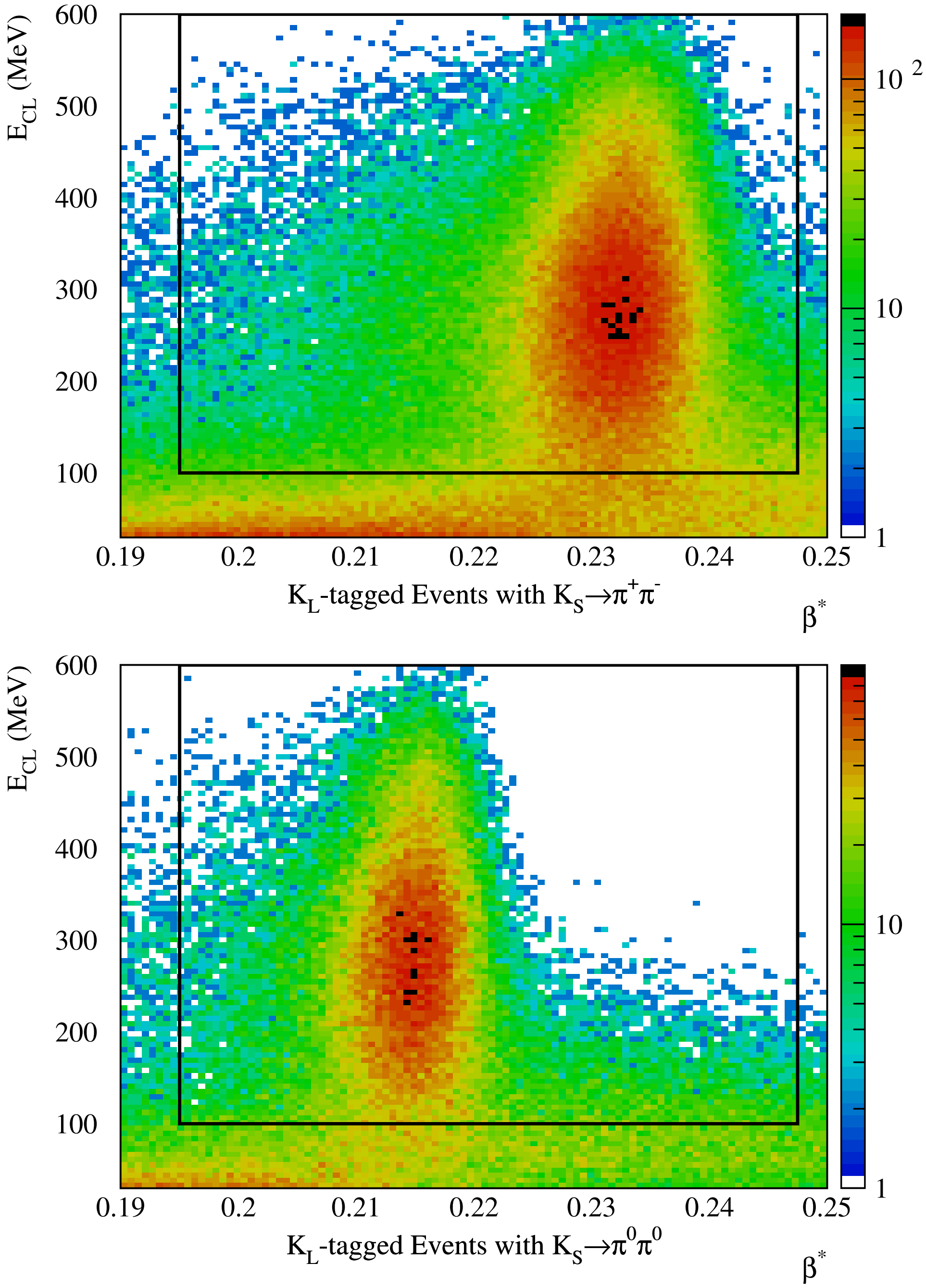

Figure 3: Distribution of the energy of the neutral clusters, as a function of the cluster velocity β^* in the ϕ rest frame, for $K_S \to \pi^+\pi^-$ (top) and $K_S \to \pi^0\pi^0$ (bottom) selected events. The applied cut is also shown. The β^* distributions peak at different values because of the different t_0 estimate.

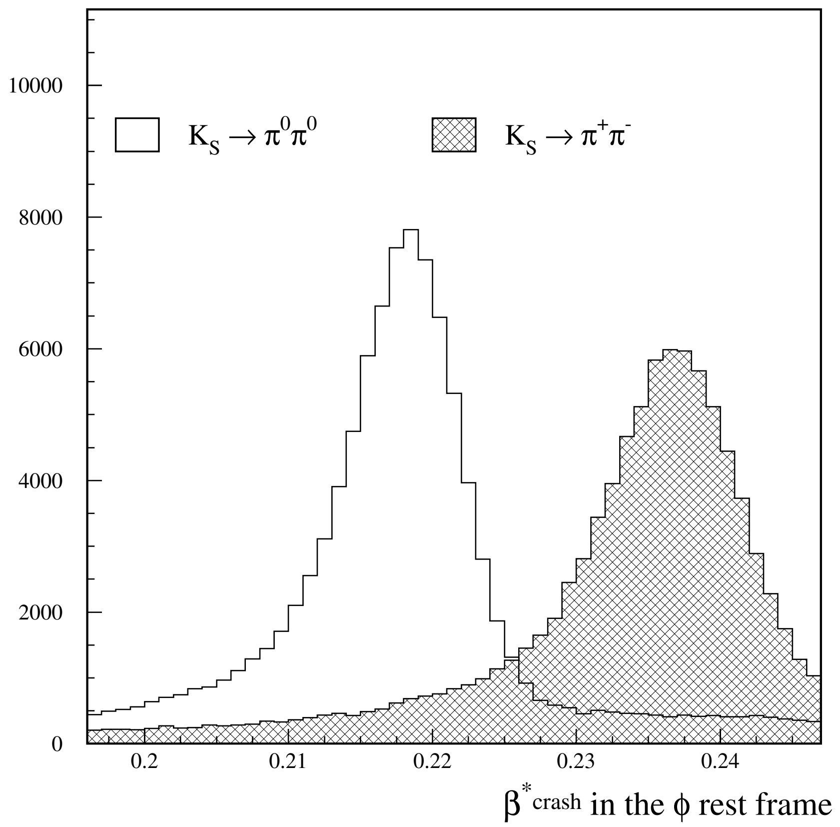

Figure 4: Distribution of neutral clusters velocity β^* in the ϕ rest frame, for $K_S \to \pi^0\pi^0$ (empty histogram) and $K_S \to \pi^+\pi^-$ events (hatched histogram), with energy above 100 MeV.

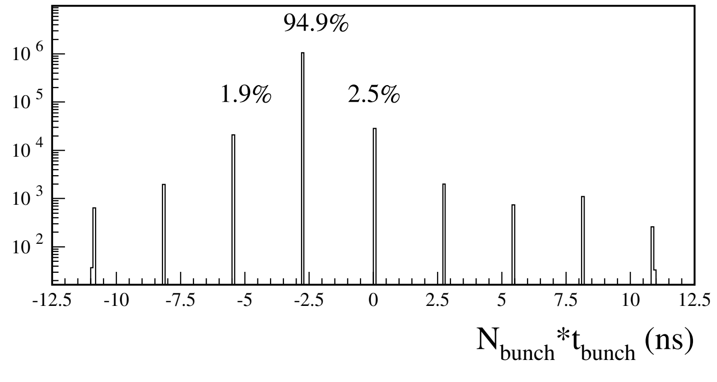

Figure 5: Distribution of the difference between the correct global-t_0 of the event and the estimated one, in $K_S \to \pi^+\pi^-$ events.

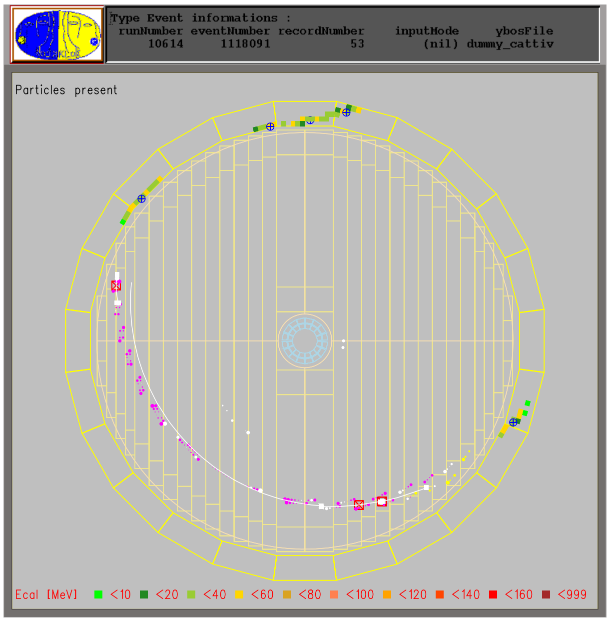

Figure 6: An example of background cosmic-ray event. The "incoming" cluster fixes the global-t_0 and the "outgoing" cluster is identified as K_{crash}.

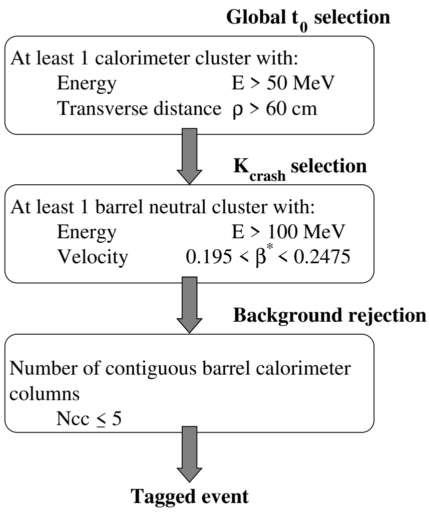

Figure 7: The K_S tag algorithm through the identification of a K_L interaction in the calorimeter.

2.3 Tag relative efficiency

The ratio of K_{crash}-tag efficiencies for the the two K_S decay modes:

$$R_{\text{tag}} = \frac{\varepsilon_{\text{crash}}\left(K_S \to \pi^+\pi^-\right)}{\varepsilon_{\text{crash}}\left(K_S \to \pi^0\pi^0\right)}$$

is needed to correct the ratio of identified events in the $\Gamma(K_S \to \pi^+\pi^-)/\Gamma(K_S \to \pi^0\pi^0)$ measurement. Three main effects can lead to a systematic difference from one of the R_{tag} ratio:

- **"t_0-efficiency"** The probability to find a t_0-cluster is different for the two decay modes. The t_0 efficiencies are not independent of the calorimeter trigger conditions and from the selection algorithms; their estimate are discussed in Sect. 5 and Sect. 10.
- **"TCA-bias"** The requirement for the K_{crash}-cluster to be neutral (not associated to any track) can, in principle, have a different effect on the two K_S decay modes: it may happens that a $\pi^\pm$ track from K_S is accidentally associated to the K_L cluster. Besides, there is a certain fraction of clusters satisfying the energy and β^* cuts, which are actually due to late K_L in flight decays. In these cases, the K_L cluster may actually be associated to a K_L track. This last effect is then expected to be independent of the K_S decay mode.

  The TCA bias effect has been estimated simply by filtering a subsample of raw events using a K_{crash}-tag in which the requirement to have a neutral cluster has been relaxed. Starting from this sample, N_{00} $K_S \to \pi^0\pi^0$ and N_{+-} $K_S \to \pi^+\pi^-$ events are selected. The same procedure is repeated with the standard K_{crash} algorithm, counting n_{00} and n_{+-} events. The TCA bias correction is therefore defined as:

$$K_{\text{TCA}} = \frac{n_{+-}}{N_{+-}} / \frac{n_{00}}{N_{00}} = (99.8 \pm 0.2)\,\%$$

- **"t_0-bias"** In events in which a t_0-cluster is found, the estimated t_0 is different with respect to the correct one. This error is different for the two decay modes. This leads to a difference in the β^*spectra (see Fig. 4), which reflects into different acceptances for a fixed β^*-window. The ratio of the acceptances of the β^*-window can be estimated directly from data, as explained in the following section.

2.4 t_0-bias

The analysis of Monte Carlo $K_S \to \pi^0\pi^0$ events shows that the t_0 estimate is the correct one at the 10^{-3} level. For $K_S \to \pi^+\pi^-$ events, the *TOSTEP0* estimate with the photon hyphotesis is compared to a more refined one, which takes into account the flight time of the K_S pions. Starting from a sample of $K_S \to \pi^+\pi^-$ events selected with the *kltag* algorithm, both pion tracks are extrapolated to the calorimeter and associated to a cluster by the track-to-cluster (TCA) algorithm. Then the global-t_0 is estimated again through Eq. (3) using the time of the cluster t_{t0CL} and the *correct* pion time-of-flight:

$$t^{\text{TOF}} = \frac{L}{c \cdot \beta_\pi}$$

where L is the total track length from the K_S vertex to the calorimeter and β_π is the velocity calculated using the track momentum and the pion mass hypothesis; the t_0^G estimates of the two pions have to be the same.

The $K_{\rm crash}$-tag is finally performed on this sample using both the t_0^G estimate in the photon hyphotesis and the refined one in the pion hyphotesis: the β^* distribution obtained using the π-t_0 in $K_S \to \pi^+\pi^-$ events should then reproduce the one of $K_S \to \pi^0\pi^0$ events, *if the selected $K_{\rm crash}$-cluster is always a K_L product, independent of the K_S decay mode* (Fig. 8).

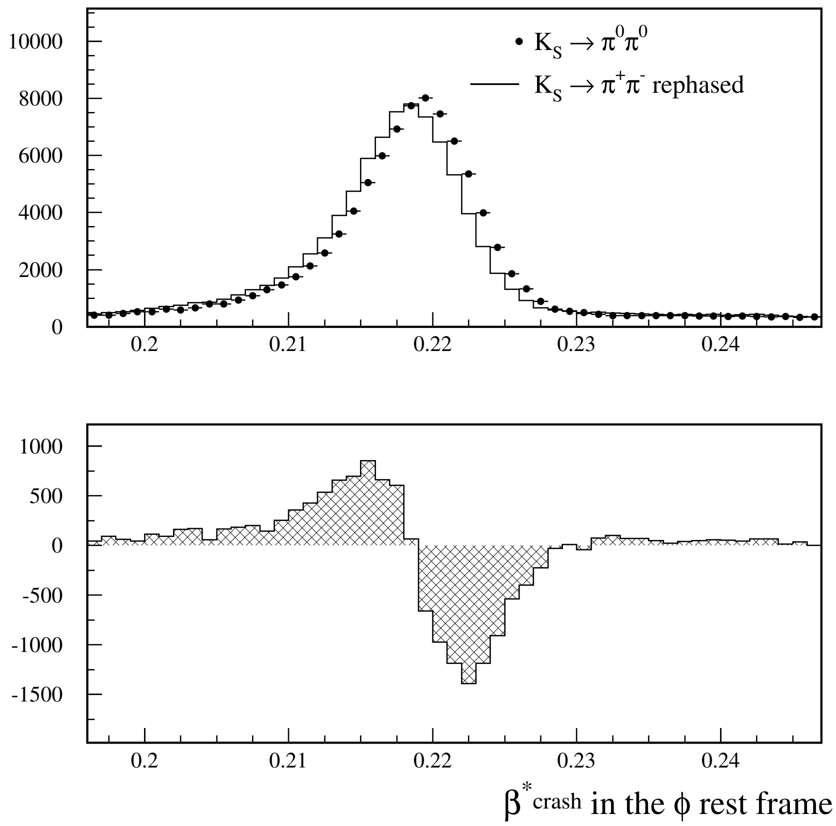

Figure 8: Comparison of the β^* distribution obtained in $K_S \to \pi^0\pi^0$ events using a photon-t_0 and in $K_S \to \pi^+\pi^-$ "rephased" events, where a pion-t_0 has been used (top). The difference of the two distributions is also shown.

If this hypothesis is correct, the ratio of tagging efficiencies can be estimated by using the number of $K_S \to \pi^+\pi^-$ events with the π-t_0, estimated with the correct TOF ($K_S \to \pi^+\pi^-$ "rephased"), in place of the $K_S \to \pi^0\pi^0$ tagged events:

$$\frac{\%\text{ of } K_S \to \pi^+\pi^-,\text{ using } \gamma\text{-}t_0}{\%\text{ of } K_S \to \pi^0\pi^0,\text{ using } \gamma\text{-}t_0} = \frac{\#\text{ of } K_S \to \pi^+\pi^-,\text{ using } \gamma\text{-}t_0}{\#\text{ of } K_S \to \pi^+\pi^- \text{ using } \pi\text{-}t_0}$$

In the right-side the *ratio of efficiencies* is replaced by the *ratio of numbers* of $K_S \to \pi^+\pi^-$ events in the two t_0 hyphoteses: this is possible since the same sample of $K_{\rm crash}$-tagged events is used. The counting of events is finally performed in the β^*-window defined for the analysis:

$$R_{tag} = \frac{\int_{\beta_{\rm min}}^{\beta_{\rm max}} f\left(\beta^*\right)\ {\rm d}\beta^*\Big|_{\pm}}{\int_{\beta_{\rm min}}^{\beta_{\rm max}} f\left(\beta^*\right)\ {\rm d}\beta^*\Big|_{\pm\pi-{\rm t}_0}}.$$

The β^*-window for the $K_{\rm crash}$ algorithm (see scheme in Fig. 7), was indeed optimized on year 1999 dataset, by minimizing the variation of the tag ratio [5]. These limits were applied at the streaming level for the year 2000 data taking.

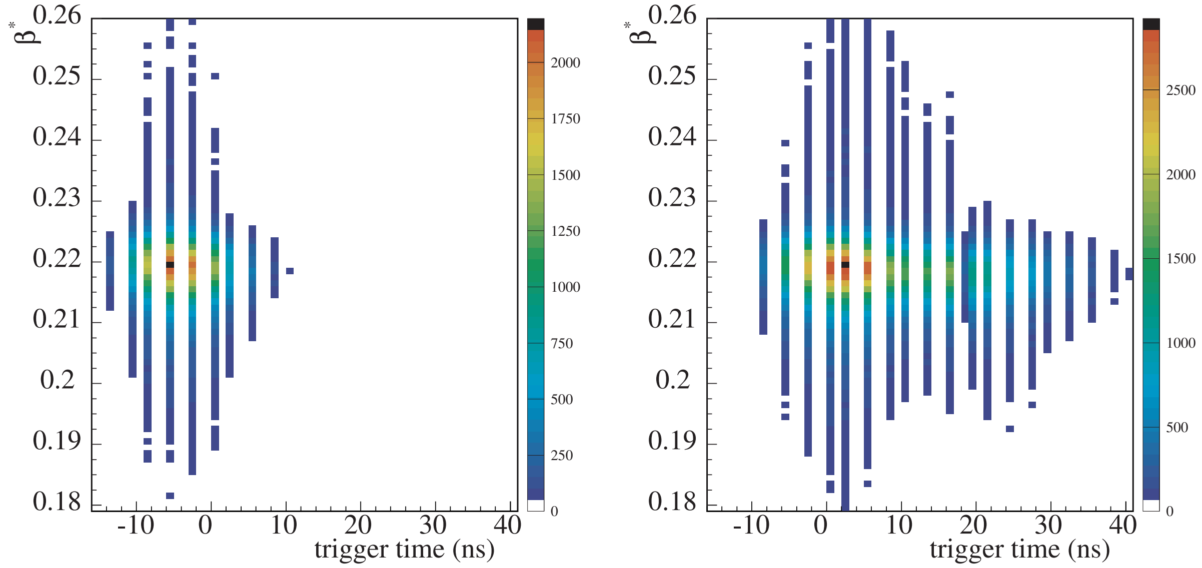

Figure 9: Events of Summer 2000 data taking. The β^* variable is shown as a function of the trigger formation time for $K_S \to \pi^0\pi^0$ (left) and $K_S \to \pi^+\pi^-$ (right) events.

Due to $\sqrt{s}$ variations and problems with the setting of the absolute time scale of the calorimeter (discussed below), a more conservative approach would have been preferable. In the year 2001 data taking a wider window has been used in the streaming phase and the fine tuning of the limits has been left to the offline analysis.

In order to study the systematics deriving from this approach, a careful comparison has been carried out between the β^* distribution obtained in $K_S \to \pi^+\pi^-$ events "rephased" using the pion-t_0 and the one of $K_S \to \pi^0\pi^0$ events, for different subsamples of the year 2000 dataset. In Fig. 8 the difference of the two distributions is shown, after having normalized them to a wider interval with respect to the window cut. The existence of a shift in the β^* distributions is evident.

Since the distribution is shifted as a *whole*, this is most likely due to an error in the absolute time scale of the events: the trigger time distribution, which determines the values of the raw calorimeter times, is in fact different for $K_S \to \pi^0\pi^0$ and $K_S \to \pi^+\pi^-$ events, as shown in Fig. 9. In the first case the sectors fired by the K_S photons are sufficient to trigger the event, while in the latter, in $\sim 40\%$ of the events the trigger has to wait 30 ns for the sectors hit by the $K_{\rm crash}$ to be satisfied.

In order to study this problem, the dependence of the β^* distribution on the formation time of the first level trigger has been studied. In each slice of the trigger time, the β^* distributions of $K_S \to \pi^0\pi^0$ and $K_S \to \pi^+\pi^-$ events have been fit to a Gaussian in a 2σ region around the peak (Fig. 10). The mean values of β^* distribution show clearly a linear slope (solid circles), which is the same for both K_S decay modes.

Correcting the absolute calorimeter times by a $(1 + 8 \times 10^{-3})$ factor, the dependence on the trigger time is flattened, as shown in the same Fig. 10 (open circles). This scale correction factor has been independently determined in the analysis of $e^+e^- \to \gamma\gamma$ events, which are used to calibrate the time scale run-by-run, just taking into account and correcting for the residual slewing [9]. A single scale factor can be used for all events of the year 2000 data taking, as shown in Fig. 11.

The β^* distributions obtained using the corrected times are shown in Fig. 12. The

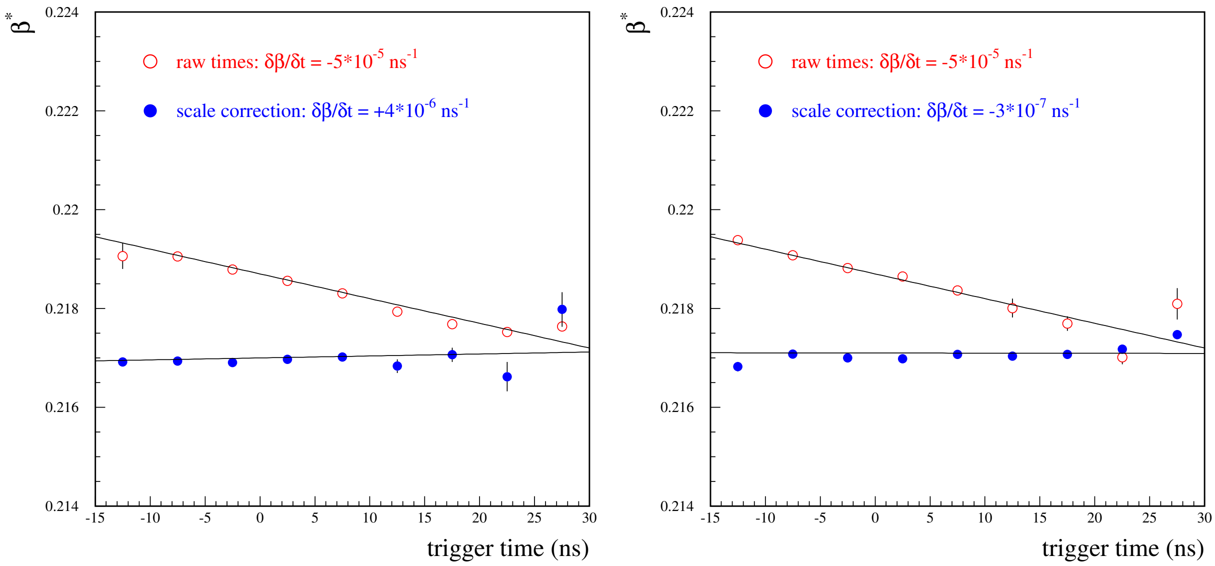

Figure 10: Events of Summer 2000 data taking. The mean values of the β^* distribution obtained through a Gaussian fit (solid circles) are shown as function of the trigger time, for $K_S \to \pi^0\pi^0$ (left) and $K_S \to \pi^+\pi^-$ (right) events. A linear fit is superimposed. The open circles are obtained correcting the absolute time scale by a factor of $(1 + 8 \times 10^{-3})$.

systematic error Δ on the ratio of tag efficiencies is estimated by calculating the ratio of the integrals of the $K_S \to \pi^+\pi^-$-*rephased* and the $K_S \to \pi^0\pi^0$-*normalized* spectra in the chosen β^*-window:

$$\Delta = 1 - \frac{\left.\int_{\beta_{\min}}^{\beta_{\max}} f\left(\beta^*\right)\ \mathrm{d}\beta^*\right|_{\pi^+\pi^-}}{W \times \left.\int_{\beta_{\min}}^{\beta_{\max}} f\left(\beta^*\right)\ \mathrm{d}\beta^*\right|_{\pi^0\pi^0}}$$

Any difference in the shape of the two distributions can affect the Δ value. The weight W, which normalizes the $K_S \to \pi^0\pi^0$ distribution of β^* to the same number of K_{crash}-interactions of the $K_S \to \pi^+\pi^-$ one, has to be determined. This normalization is a crucial point, since it is influenced by any significant difference in the tails of the two distributions.

The factor W has been determined by fitting with a constant the ratio bin-by-bin of the two distributions (Fig. 13). This is repeated for different fit intervals around the β^* peak. Any deviation of the fit constant signals a difference in the tails of the two distributions, as can also be seen from the χ^2-values. If the value of W shows such a dependence, as for the October-November 2000 subsample, the tails are excluded by choosing the normalization at $\pm 2\sigma$ from the peak.

The difference in the tails between the Summer 2000 and October-November 2000 subsamples is due to a different value of $\sqrt{s}$ in the two running periods that shifts the peak with respect to the β^*-window. This reflects in a different relative weight of the tails. These tails are mainly due to pion fragments in $K_S \to \pi^+\pi^-$ events, as shown in Fig. 14, where they appear as a diffuse background.

Since the spectrum of the pion fragments is peaked at low energy, their contribution in the K_{crash} events can be reduced by increasing the 100 MeV cut in the K_{crash} selection. In order to reduce the systematic error, this energy cut has been varied and the tag efficiency ratio has been calculated for each value, as shown in Fig. 15; the systematic error has been evaluated by normalizing the $K_S \to \pi^0\pi^0$ distribution with the W factor from a $\pm 2\sigma$-fit of the bin-by-bin ratio. The cut has been tuned by minimizing the estimated systematic

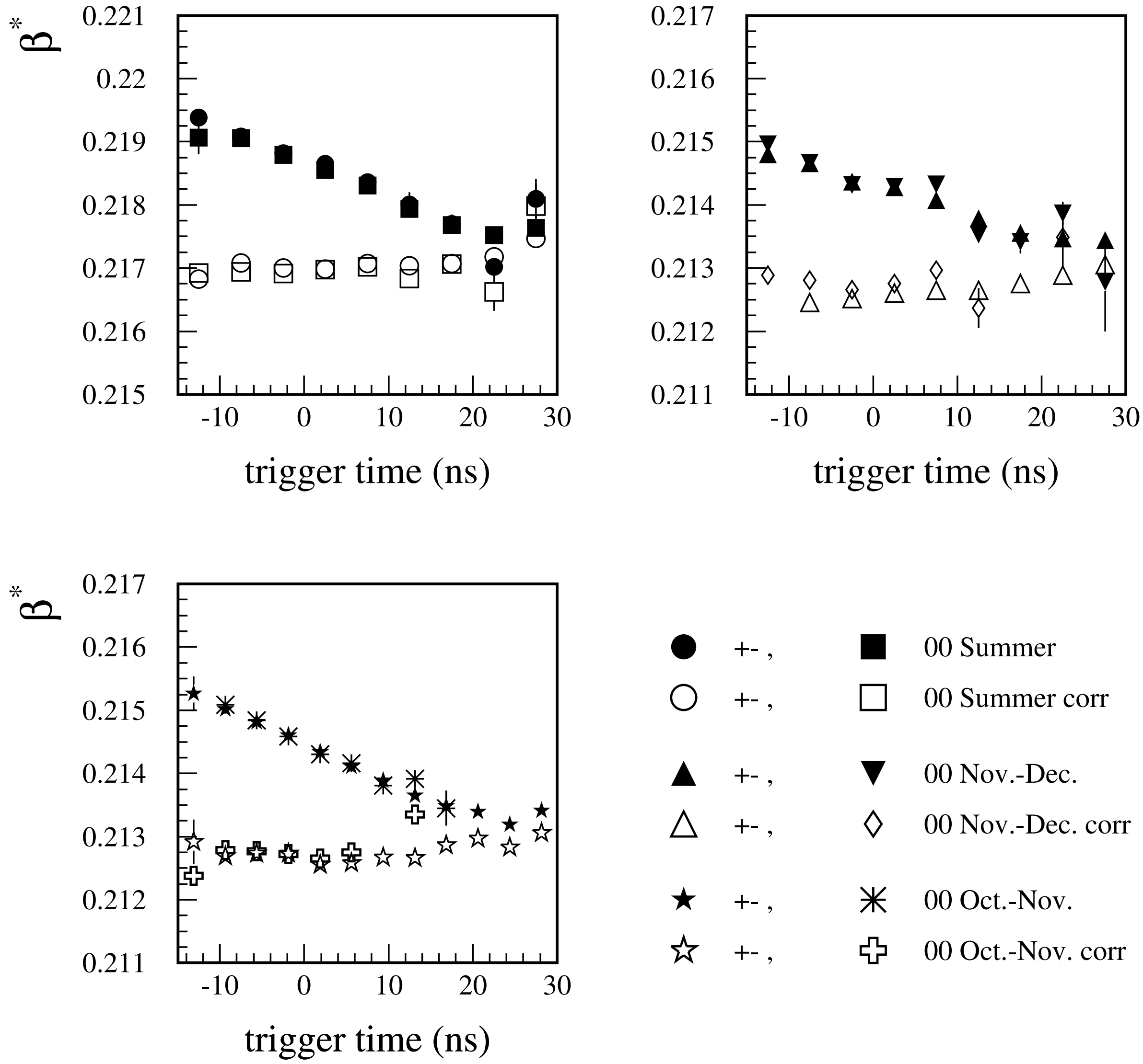

Figure 11: Events of the year 2000 data taking. The mean of the β^* distribution is shown as a function of the trigger time, as calculated using raw (solid symbols) and corrected (open symbols) calorimeter times, for $K_S \to \pi^0\pi^0$ and $K_S \to \pi^+\pi^-$. Different run periods are distinguished: Summer 2000, Oct.-Nov. 2000, and Nov.-Dec. 2000.

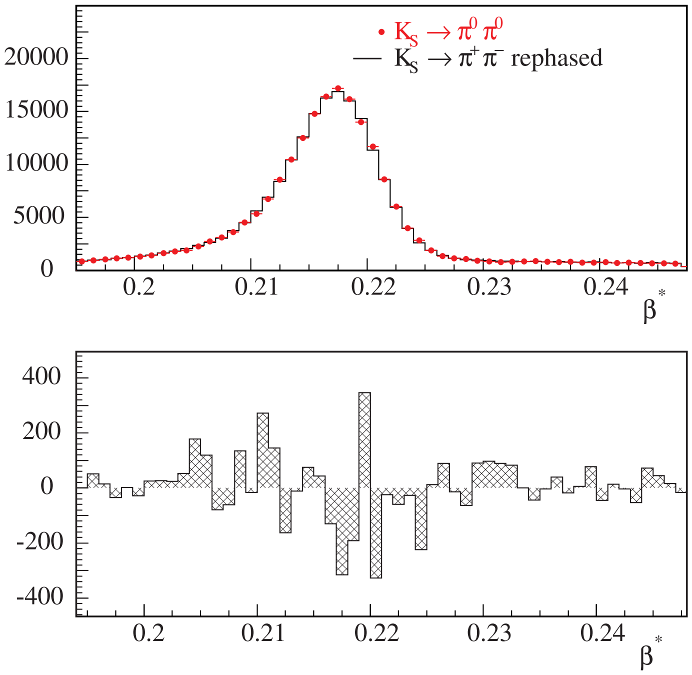

Figure 12: Events of Summer 2000 data taking. (Top) The β^* variable is shown as calculated using corrected calorimeter times, for $K_S \to \pi^0\pi^0$ (solid circles) and $K_S \to \pi^+\pi^-$ with pion-t_0 (solid line) events. (Bottom) Difference of the upper distributions, normalized as explained in the text.

error versus its statistical error, as shown in Fig. 16 (see discussion in Sect. 12).

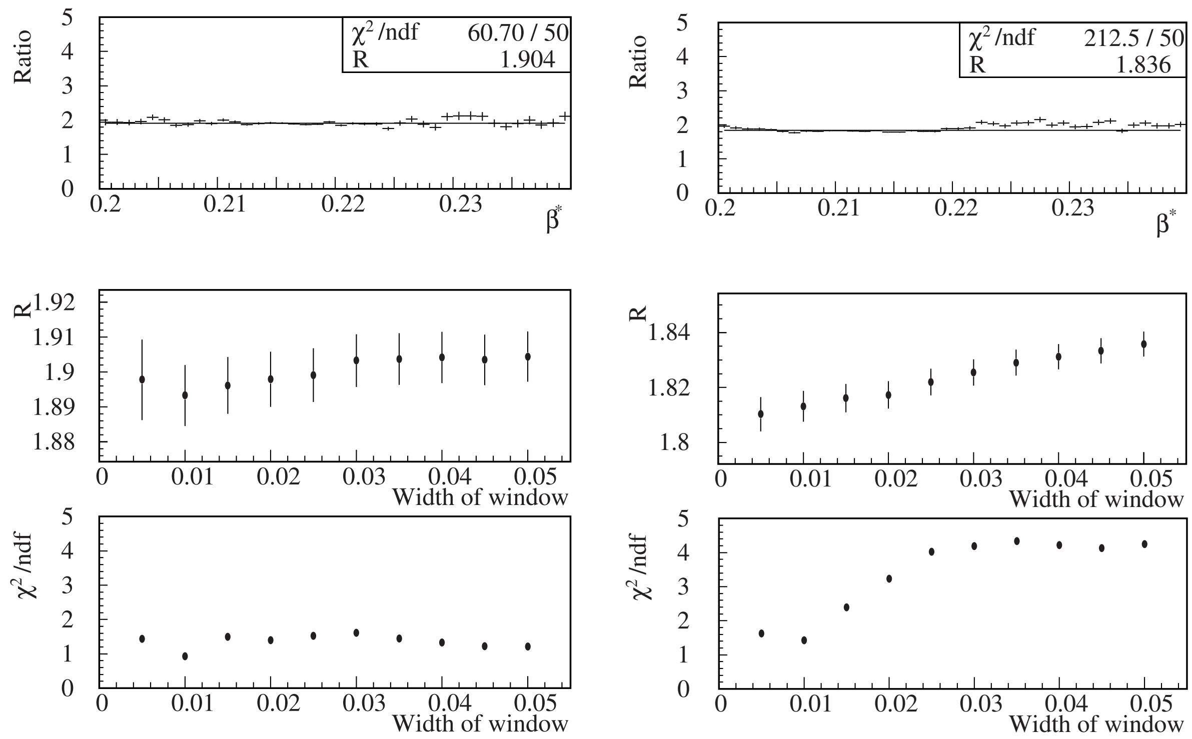

Figure 13: Events of Summer 2000 (left) and October-November 2000 (right) data taking. In the upper plots the ratio bin by bin of the distributions of $K_S \to \pi^+\pi^-$ obtained using pion-t_0 and $K_S \to \pi^0\pi^0$ is shown as a function of the β^* variable. The result of the fit to a constant R is shown as function of the width of the fit interval, centered around the peak. The χ^2-value of the fits, normalized to the number of degrees of freedom, is also shown in the lower plots.

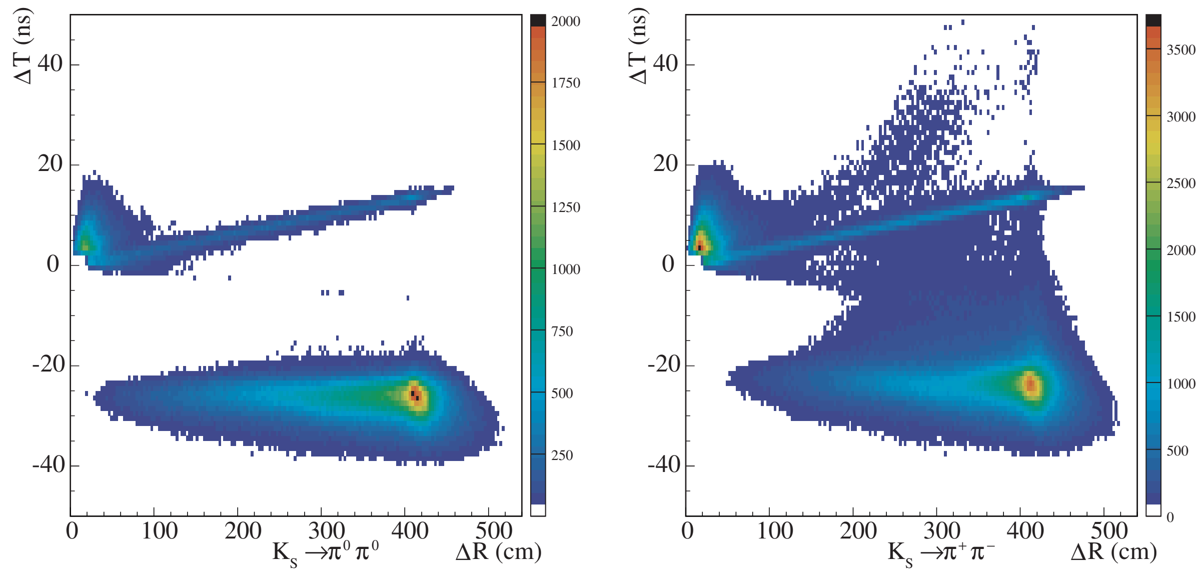

Figure 14: Events of November 2000 data taking. The time difference and the space distance with respect to the K_{crash} clusters are plotted for $K_S \to \pi^0\pi^0$ (left) and $K_S \to \pi^+\pi^-$ (right) events. In the plots there is one entry per cluster of energy above 100 MeV (the K_{crash} cluster is excluded).

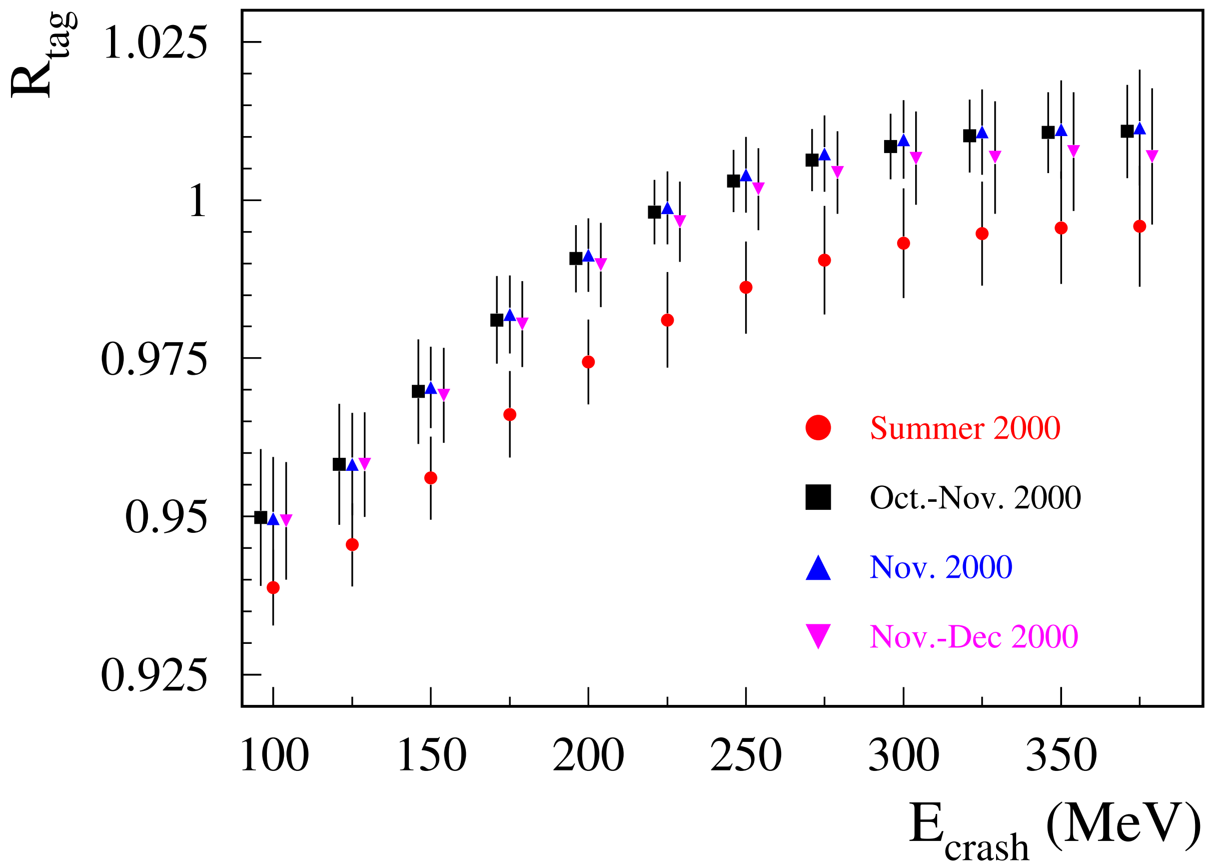

Figure 15: Events of 2000 data taking. Ratio of tagging efficiencies, calculated using the $K_S \to \pi^+\pi^-$ sample only, as a function of the K_{crash}-energy cut. The year 2000 statistics has been divided into four subsamples. The difference between the Summer sample and the others is mainly due to the $\sqrt{s}$ value.

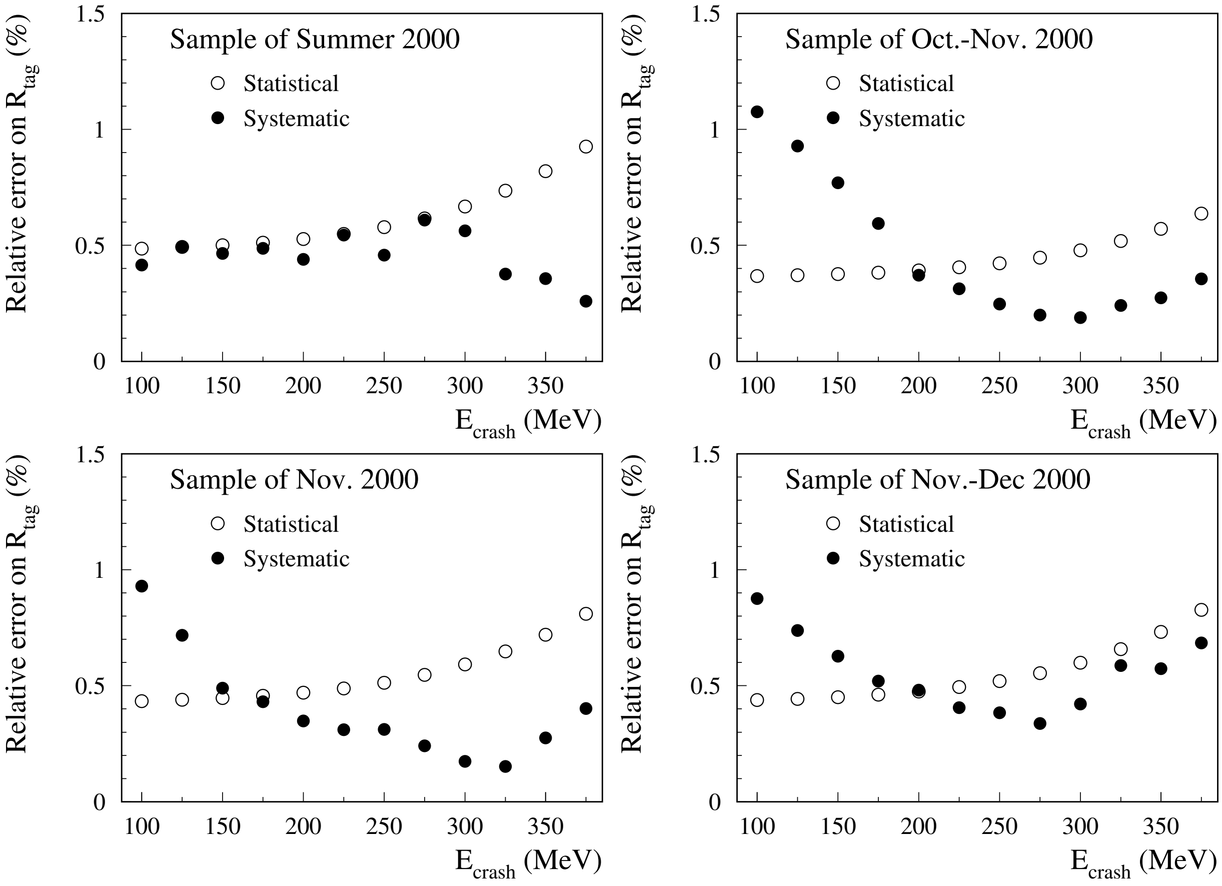

Figure 16: Events of 2000 data taking. The systematic error on the ratio of tagging efficiencies is shown as a function of the $K_{\rm crash}$ energy cut, together with its statistical uncertainty. The Summer, October-November, November-December and December 2000 samples are shown separately.

3 Selection of $K_S \to \pi^0\pi^0$ events

The $K_S \to \pi^0\pi^0$ selection is based on the identification of prompt photon clusters from the π^0 decays. Only neutral clusters, not associated to any track by the TCA algorithm, are considered. The photon identification is performed using neutral cluster-centroid times ($t_{\rm CL}$) after having subtracted the global-t_0, as discussed in Sect. 2.1. A neutral cluster is called "prompt" if its time-of-flight satysfies a 5σ cut:

$$|t_{\rm CL} - |\mathbf{r}_{\rm CL}|/c| \leq 5 \cdot \sigma_{\rm t}(E_{\rm CL})$$

where the parametrization of the resolution in the cluster time

$$\sigma_{\rm t}(E_{\rm CL}) = \frac{57 \text{ ps}}{\sqrt{E_{\rm CL}\,[\text{GeV}]}} \oplus 140 \text{ ps}$$

has been obtained using a selected photon sample from $\phi \to \pi^+\pi^-\pi^0$ events (Sect. 4).

In order to minimize the probability that an accidental cluster is counted as a photon, clusters in the region of soft energy and low polar angles are not considered:

$$E_{\rm CL} \geq 20 \text{ MeV}$$

$$|\cos\theta_{\rm CL}| \leq 0.9 \Longleftrightarrow 25.8° \leq \theta_{\rm CL} \leq 154.2°$$

The distribution of the number $N_{\rm prompt}$ of accepted neutral prompt clusters from $K_{\rm crash}$-

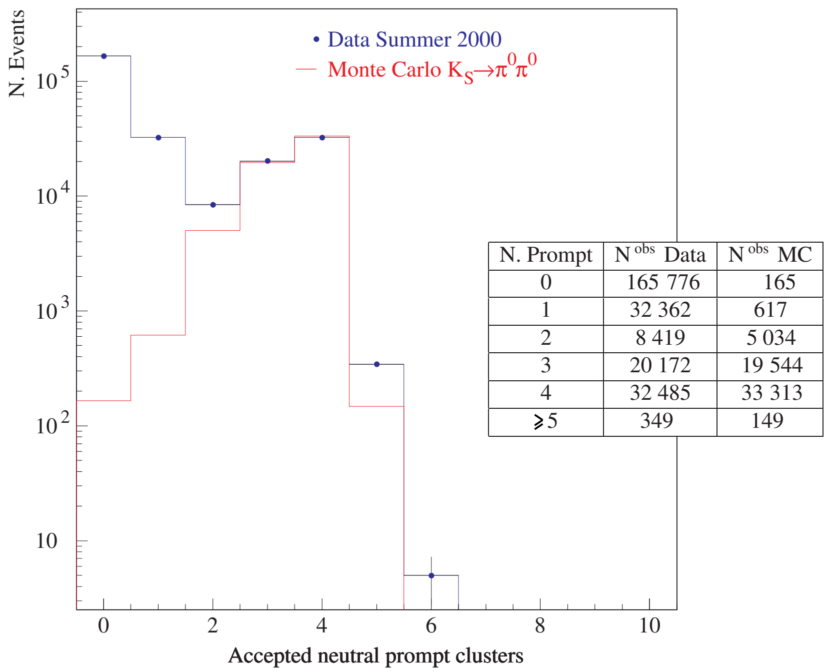

N. Prompt	N^{obs} Data	N^{obs} MC
0	165 776	165
1	32 362	617
2	8 419	5 034
3	20 172	19 544
4	32 485	33 313
⩾5	349	149

Figure 17: Distribution of the number of neutral prompt clusters from $K_{\rm crash}$-tagged events of the Summer-2000 data taking (circles) and from $K_S \to \pi^0\pi^0$ Monte Carlo events (line). The Monte Carlo distribution has been scaled to the same number of events with three or more selected clusters. The corresponding number of events are listed in the table.

tagged events of the Summer 2000 data taking is shown in Fig. 17 compared to Monte Carlo $K_S \to \pi^0\pi^0$ events. Monte Carlo events were obtained by tuning the simulation using data-extracted efficiencies (Sect. 4). The data and Monte Carlo distributions are normalized to the same number of events with three or more selected clusters, which are background-free (Sect. 6).

Referring to Fig. 17, the discrepancy in the population of the events with $N_{\text{prompt}} = 0, 1, 2$ prompt clusters is mainly due to $K_S \to \pi^+\pi^-$ events and background events (cosmic-ray and machine-background). In $K_S \to \pi^+\pi^-$ events, in fact, the track-to-cluster association can fail for one or both pion tracks; the resulting "neutral" cluster appears to be prompt, since the global-t_0 is fixed by the cluster itself.

The discrepancy in the bins with $N_{\text{prompt}} = 5, 6$ is not due to the background. Two conspiring effects are present: the contamination (only in data) of accidental clusters surviving the imposed cuts, and a difference in the data and Monte-Carlo of the "splitting" probability. This is the probability of producing more than one selected cluster for each incident photon; in general the splitting results in a "main" cluster surrounded by one or more low energy fragments. The effect of the splitting can be clearly seen in the five prompt sample, selected with a lower energy cut ($E_{\text{cut}} = 7$ MeV). In Fig. 18 the minimum-distance pair of prompt clusters is selected and the minimum distance is plotted as a function of the minimum energy in the pair.

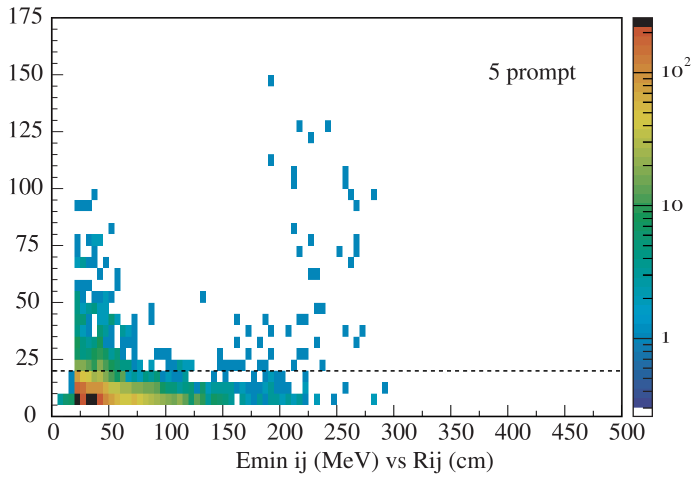

Figure 18: Events selected using the K_{crash}-tag with five prompt neutral clusters, imposing an energy cut $E_{\text{CL}} \geq 7$ MeV. Among all the pairs of selected clusters, that with minimum distance is taken and the minimum distance is shown vs. the minimum energy of the pair. The 20-MeV energy cut is also shown by the dashed line.

The peak at low energy and distance is due to split clusters. The accidental clusters populate the low energy region, too. Both effects result in letting events with four (three) incident photons give five (four) selected clusters, and can be partially reduced by applying the 20-MeV energy cut; the residual effect can be seen by comparing data and Monte Carlo energy and polar-angle distributions for events with $N_{\text{prompt}} = 3, 4, \geq 5$ prompt clusters (Fig. 19). Data and Monte Carlo energy and angular spectra are in good agreement at least for the three and four prompt cluster events, while different behaviors are observed in events with five or more clusters. For low energies both the cited different splitting probability and the presence in data of accidental clusters can contribute; these two effects can be instead distinguished in the region $|\cos\theta| > 0.6$: while the peaks in the angular region corresponding to the separation between barrel and end-cap are mainly due to split

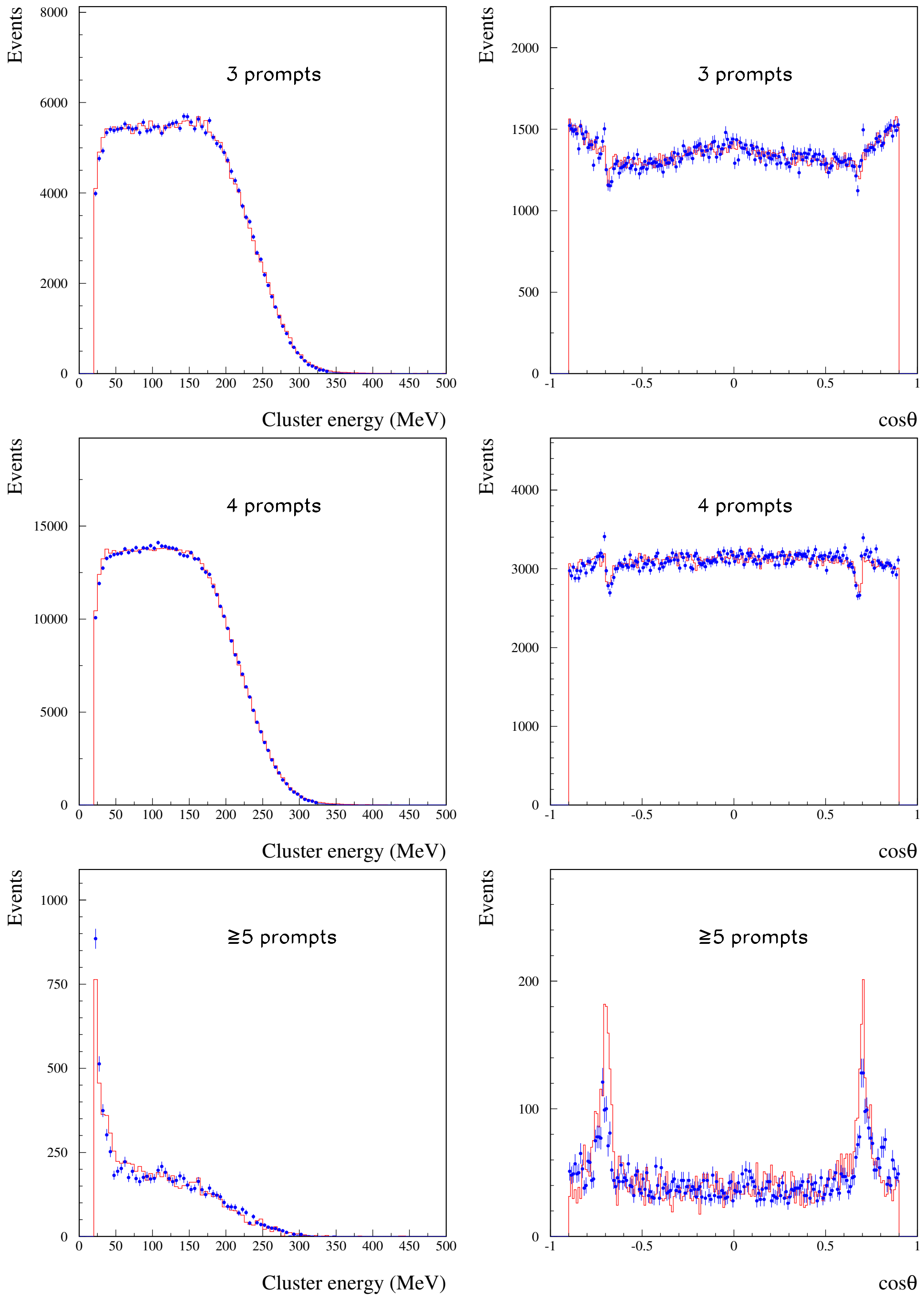

Figure 19: Distributions of the energies (left) and polar angle (right) of the neutral prompt clusters from $K_{\rm crash}$-tagged events of the Summer-2000 data taking (circles) and from $K_S \to \pi^0\pi^0$ Monte Carlo events (solid line). Events with three, four, and more than four selected clusters are separately plotted in the top, center, and bottom panels respectively. Data and Monte Carlo distributions are normalized above 50 MeV.

clusters, for very low angles the contribution of the accidental clusters is dominant.

The signal selection is finally performed by applying an inclusive cut:

$$N_{\text{prompt}} \geq N_{\text{min}}$$

Both thresholds values $N_{\text{min}} = 3$ and $N_{\text{min}} = 4$ could be used to select a background-free sample (as discussed in Sect. 6); the acceptance is evaluated from Monte Carlo: $\varepsilon_{N\geq 3} \simeq 90.1\%$, $\varepsilon_{N\geq 4} \simeq 56.9\%$. Even though a larger efficiency would be welcome, the systematics have to be taken into account. The main contributions to the systematic error come from the difference of the splitting probabilities in data and Monte Carlo, the contamination from accidentals clusters (not included in the simulation), and the accuracy of the Monte Carlo in reproducing the real photon detection efficiency.

While the photon detection efficiency is discussed in Sect. 4.3, here the systematic errors due to splitting and accidentals are evaluated:

- **Accidentals** The probability $P_{\text{A}}(1)$ that a *single* accidental cluster above 20 MeV enters the 5σ promptness window is measured directly from cosmic-ray data: $P_{\text{A}}(1) \sim 2 \times 10^{-3}$. The probability to have *two* accidentals in the same window is $P_{\text{A}}(2) \sim 0.5 \times 10^{-3}$. The number $N^{\text{obs}}_{\geq 3(4)}$ of observed events with more than three (four) prompt is related to the distribution $\{n_{\text{i}}\}$ in absence of accidentals, as follows:

$$\begin{aligned} N^{\text{obs}}_{\geq 3} &= n_1 \cdot P_{\text{A}}(2) + n_2 \cdot P_{\text{A}}(1) + n_{\geq 3} \\ N^{\text{obs}}_{\geq 4} &= n_2 \cdot P_{\text{A}}(2) + n_3 \cdot P_{\text{A}}(1) + n_{\geq 4} \end{aligned}$$

  Since the P_{A} probabilities are small, it is a valid approximation to evaluate the right hand side using the number of observed events of Fig. 17 in place of n_{i}. The fractional variations are:

$$\frac{N_{\geq 3} - n_{\geq 3}}{n_{\geq 3}} \sim 0.6 \times 10^{-3}$$
$$\frac{N_{\geq 4} - n_{\geq 4}}{n_{\geq 4}} \sim 1.4 \times 10^{-3}$$

  The above differences are an estimate for this contribution to the relative systematic error.
- **Splitting** The probability P_{S} for a single incident photon to produce two prompt clusters is estimated from data, by using the relation:

$$P_{\text{S}} = \frac{N_5}{4 \cdot N_4} = 2.7 \times 10^{-3} \text{ (MC value: } 1.1 \times 10^{-3}\text{)}$$

  This relation gives an overestimate of P_{S} in data, since the presence of the accidentals has not been subtracted. However, using the same approximation applied in the case of accidentals, the variations in the number of accepted events are:

$$\begin{aligned} \frac{N_{\geq 3} - n_{\geq 3}}{n_{\geq 3}} &= 2 \times P_{\text{S}} \times \frac{N_2}{N^{\text{obs}}_{\geq 3}} \sim 0.9 \times 10^{-3} \text{ (MC value: } \sim 0.2 \times 10^{-3}\text{)} \\ \frac{N_{\geq 4} - n_{\geq 4}}{n_{\geq 4}} &= 3 \times P_{\text{S}} \times \frac{N_3}{N^{\text{obs}}_{\geq 4}} \sim 5 \times 10^{-3} \text{ (MC value: } \sim 2 \times 10^{-3}\text{)} \end{aligned}$$

  Hence, the systematic error due to the splitting can be evaluated by the difference between data and Monte Carlo estimates: the relative systematic uncertainty in the acceptance of the cut $N_{\text{prompt}} \geq N_{\text{min}}$ is $\sim 0.7 \times 10^{-3}$ for $N_{\text{min}} = 3$ and $\sim 3 \times 10^{-3}$ for $N_{\text{min}} = 4$.

4 Photon detection efficiency and systematics

The neutral-prompt-cluster efficiency has been estimated in two steps. First the photon detection efficiency is extracted directly from data samples of $\phi \to \pi^+\pi^-\pi^0$ as a function of the photon energy and polar angle (Sect. 4.1), then the systematic error on this estimate is calculated (Sect. 4.2). The efficiency profiles are used to tune the Monte Carlo simulation, and the data-tuned Monte Carlo is used to calculate the efficiency of the cut on the number of neutral prompt clusters in the event (Sect. 4.3).

4.1 Photon detection efficiency

The efficiency to detect a photon cluster, passing the 5σ promptness cut has been estimated using the events classified into the "$\rho\pi$ stream". The method aims first to identify the $\pi^\pm$-clusters and one "tagging" photon cluster coming from the π^0 decay. The vector-momentum of the other "candidate" photon is then estimated by kinematically closing the event. The prompt cluster due to the candidate photon is finally searched within a cone centered around its estimated direction. The efficiency is given by the fraction of the selected events in which a candidate cluster is matched.

The selection cuts used to identify the $\phi \to \pi^+\pi^-\pi^0$ decay vertex and a *tagging* photon are summarized below:

- A charged vertex close to the interaction point is required, reconstructed by two tracks of opposite charge, both associated to calorimeter "pion" clusters.
- A 2σ cut around M_{π^0} is applied on the missing invariant mass, calculated by assigning the pion mass to both track momenta and using the values of ϕ energy and momentum, run-by-run estimated using Bhabha events:

$$\begin{aligned} E^{\rm miss}_{\pi\pi} &= \sqrt{P_\phi^2 + \sqrt{s}^2} - \sqrt{\mathbf{p}_1^2 + M_\pi^2} - \sqrt{\mathbf{p}_2^2 + M_\pi^2} \\ \mathbf{P}^{\rm miss} &= \mathbf{P}_\phi - \mathbf{p}_1 - \mathbf{p}_2 \\ M^{\rm miss} &= \sqrt{(E^{\rm miss}_{\pi\pi})^2 - |\mathbf{P}^{\rm miss}|^2} \end{aligned}$$

- In order to avoid a bias on the photon detection efficiency, the selection of the tagging photon has not to depend on its energy. Therefore, the photon energies are estimated in the π^0 rest frame making use of the missing momentum measured by the chamber and of the cluster *direction* only. The boost parameters are obtained by assigning the π^0 mass to the missing momentum $\mathbf{P}^{\rm miss}$, and, for each neutral cluster with a position vector $\mathbf{r}_{\rm CL}$ with respect to the selected vertex, the "DC energy" is calculated:

$$\begin{aligned} \gamma &= \frac{\sqrt{M_{\pi 0}^2 + |\mathbf{P}^{\rm miss}|^2}}{M_{\pi 0}} \\ E_{\rm DC} &= \frac{\gamma}{2} \times M_{\pi 0} \frac{1 + \beta \cdot (-\beta + \cos\alpha)}{1 - \beta\cos\alpha} \end{aligned}$$

  where $\cos\alpha = \hat{\mathbf{r}}_{\rm CL} \cdot \hat{\mathbf{P}}^{\rm miss}$. Since $E_{\rm DC}$ is a good estimator of the "true" photon energy, at the level of σ =1 MeV, the cluster energy resolution $\sigma_{\rm E}$, the time resolution $\sigma_{\rm T}$, and the effective slewing $\mu_{\rm T}$[1)] can be parametrized using data (see [10]).

[1)] Namely the mean value of the difference between the measured and expected cluster time.

The final selection of the tagging photon is performed using a χ^2-like variable, calculated for each *single* neutral cluster:

$$\chi^2 = \left(\frac{E_{\mathrm{CL}} - E_{\mathrm{DC}}}{\sigma_{\mathrm{E}}\left(E_{\mathrm{DC}}\right)}\right)^2 + \left(\frac{T_{\mathrm{CL}} - r_{\mathrm{CL}}/c - \mu_{\mathrm{T}}\left(E_{\mathrm{DC}}\right)}{\sigma_{\mathrm{T}}\left(E_{\mathrm{DC}}\right)}\right)^2$$

The distribution of this variable is shown in Fig. 20; tagging photons are selected requiring $\chi^2 \leq 20$.

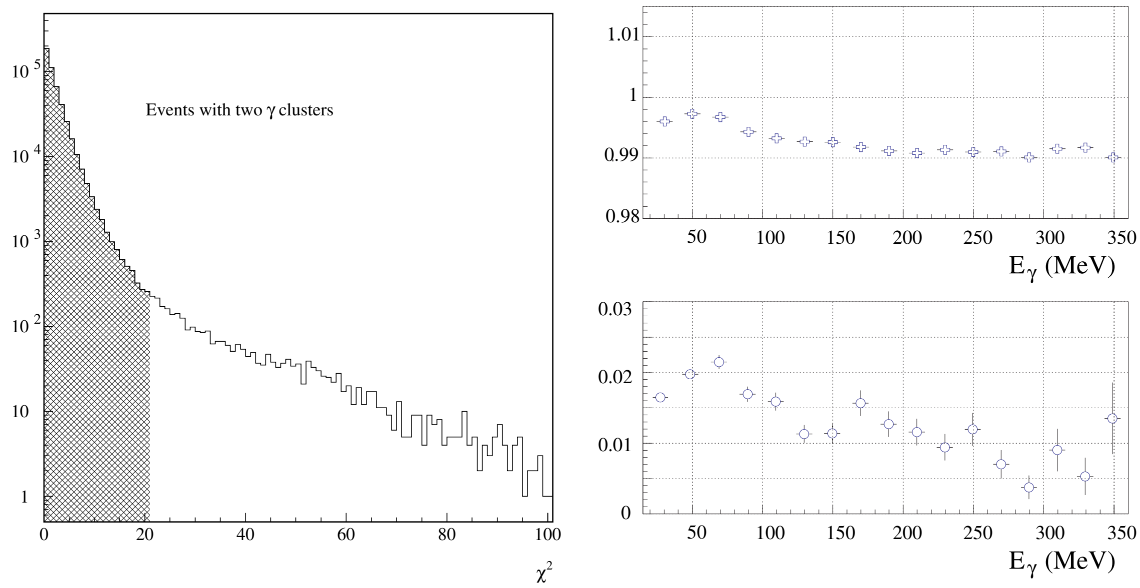

Figure 20: $\phi \to \pi^+\pi^-\pi^0$ events with two photon clusters, selected using the φ^* variable only. (Left) Distribution of the χ^2 variable (see text), for the two photon clusters. The cut used to select the single photon clusters is superimposed. (Right) Efficiency (top) and contamination (bottom) of the cut $\chi^2 \leq 20$ as a function of the expected "DC" energy of the photon.

– In order to avoid biases induced by the trigger, the conditions imposed by the calorimeter trigger have to be satisfied using *only* the trigger sectors fired by the tagging cluster together with the pion clusters, "switching off" all of the trigger sectors with a contribution from the other clusters in the event.

The momentum of the candidate photon is estimated using the direction $\hat{\mathbf{r}}_{\mathrm{CL}}$ and the calculated energy E_{DC} of the tagging photon:

$$\mathbf{P}_\gamma^{\mathrm{candidate}} = \mathbf{P}^{\mathrm{miss}} - E_{\mathrm{DC}} \cdot \hat{\mathbf{r}}_{\mathrm{CL}}$$

Finally a candidate cluster is *matched* if it is prompt and it lies within a cone centered around the estimated direction:

$$|\delta_{\mathrm{t}}| \leq 5\sigma_{\mathrm{t}}\left(E_{\mathrm{CL}}\right)$$

$$\hat{\mathbf{r}}_{\mathrm{CL}} \cdot \hat{\mathbf{P}}_\gamma^{\mathrm{candidate}} \geq \cos_{\mathrm{min}}$$

Different angular cuts $\cos_{\mathrm{min}} = 0.6, 0.7, 0.8, 0.9$ have been tried in the matching. The efficiency has been calculated as a function of the candidate photon energy, in 15-MeV bins of E_γ, and polar angle, in 60° bins of θ_γ. The photon detection efficiency is defined as:

$$\varepsilon_\gamma\left(\mathrm{E}_\gamma, \theta_{\mathrm{gamma}}\right) = \frac{\#\text{ of ev. in a } (E_\gamma \otimes \theta_\gamma)\text{-bin with a } \textit{matched candidate cluster}}{\text{Total } \#\text{ of selected ev. in a } (E_\gamma \otimes \theta_\gamma)\text{-bin}}$$

The final results for the efficiency are plotted in Fig. 21 for data of the October-2000 period of data taking. The efficiency plateau is very close to 100%, while a 15% drop is observed at 25 MeV.

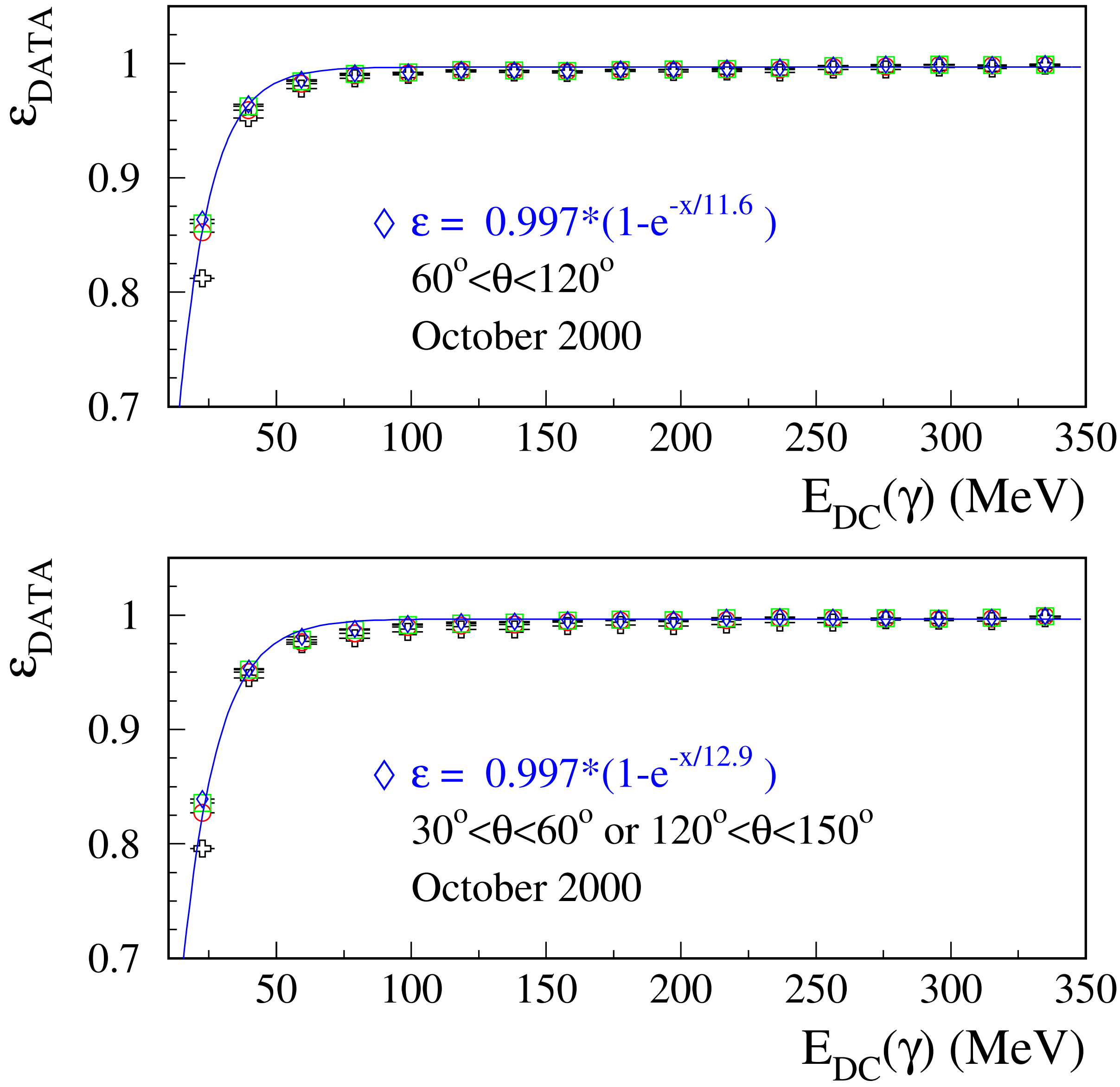

Figure 21: Photon detection efficiency profiles as a function of the expected photon energy, in 60°-slices of the photon polar angle θ, for October 2000 data taking. The different symbols correspond to the candidate-matching definitions $\cos_{\min} = 0.6, 0.7, 0.8, 0.9$.

4.2 Photon detection systematics

The efficiency estimate has been repeated using different data taking periods and also varying the χ^2 cut used to select the first photon cluster. The efficiency profiles are fit to the function:

$$\varepsilon_\gamma = P_1 \times [1 - \exp(-E_{\mathrm{DC}}/P_2)] \tag{5}$$

The efficiency of the χ^2 cut as a function of the energy is evaluated again in the events with two photon clusters (right-top of Fig. 20). These events are also used to evaluate the probability of selecting a split fragment cluster instead of the photon one (right-bottom of Fig. 20), thus giving a worse estimate of the candidate-photon momentum. The selection efficiency of the tagging photon is almost flat apart from the region below 100 MeV. This corresponds to an energy of the candidate photon above 250 MeV. Hence, in this region the estimated efficiency has a larger systematic error.

The absolute scale of the missing mass distribution has to be checked, in order not to bias the photon energy estimate: therefore run-by-run values of the ϕ momentum and energy have been then used in the calculation. The mean value of M^{miss}, plotted as a function of the run period in Fig. 22, does not show appreciable variations, apart from statistical fluctuations. The efficiency results are proved to be stable at the level of few

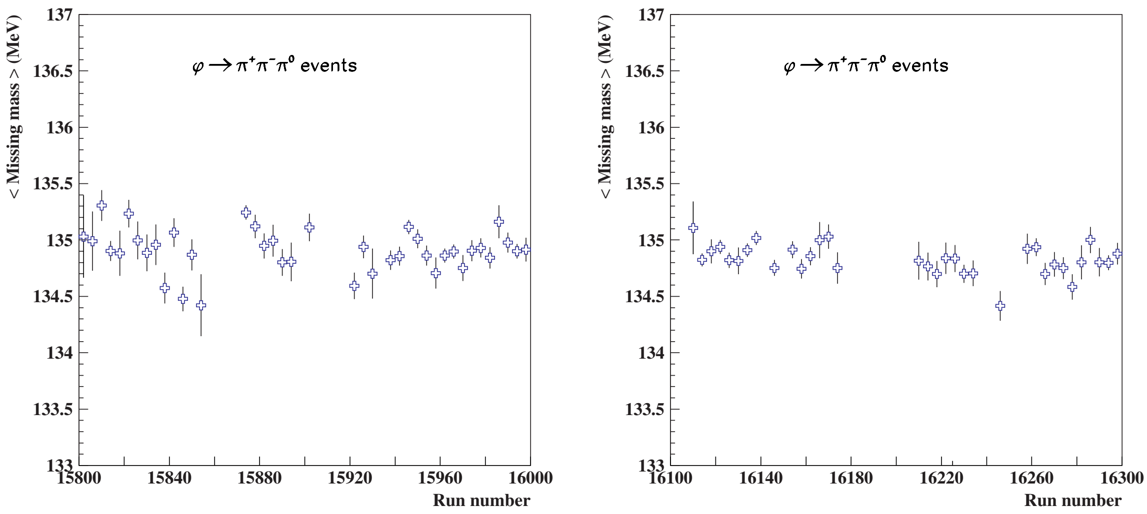

Figure 22: The mean value of the missing mass, derived from a Gaussian fit, is shown as function of the run period for data of the year 2000: 16/10–22/10 (left) and 27/10–2/11 (right).

10^{-3}.

4.3 Systematic error on the Monte Carlo efficiency

The efficiency estimate has been performed also using Monte Carlo events $\phi \to \pi^+\pi^-\pi^0$. The data/Monte Carlo ratio can be optimized by tuning the effective energy threshold (in the Monte Carlo) for an hit cell to be reconstructed and connected to a cluster. In Fig. 23, this ratio is plotted as a function of the energy and polar angle of the photon, where a first correction to the Monte Carlo threshold has been applied. The fits to the function (5) are superimposed. The agreement is good at the percent level, except for the low-energy region, below 50 MeV. This is due to a residual difference in the energy response between data and Monte Carlo. Even though a finer tuning of the energy simulation is still in progress, the effect of the data-Monte Carlo difference of the photon detection efficiency on the prompt-cluster counting can be estimated.

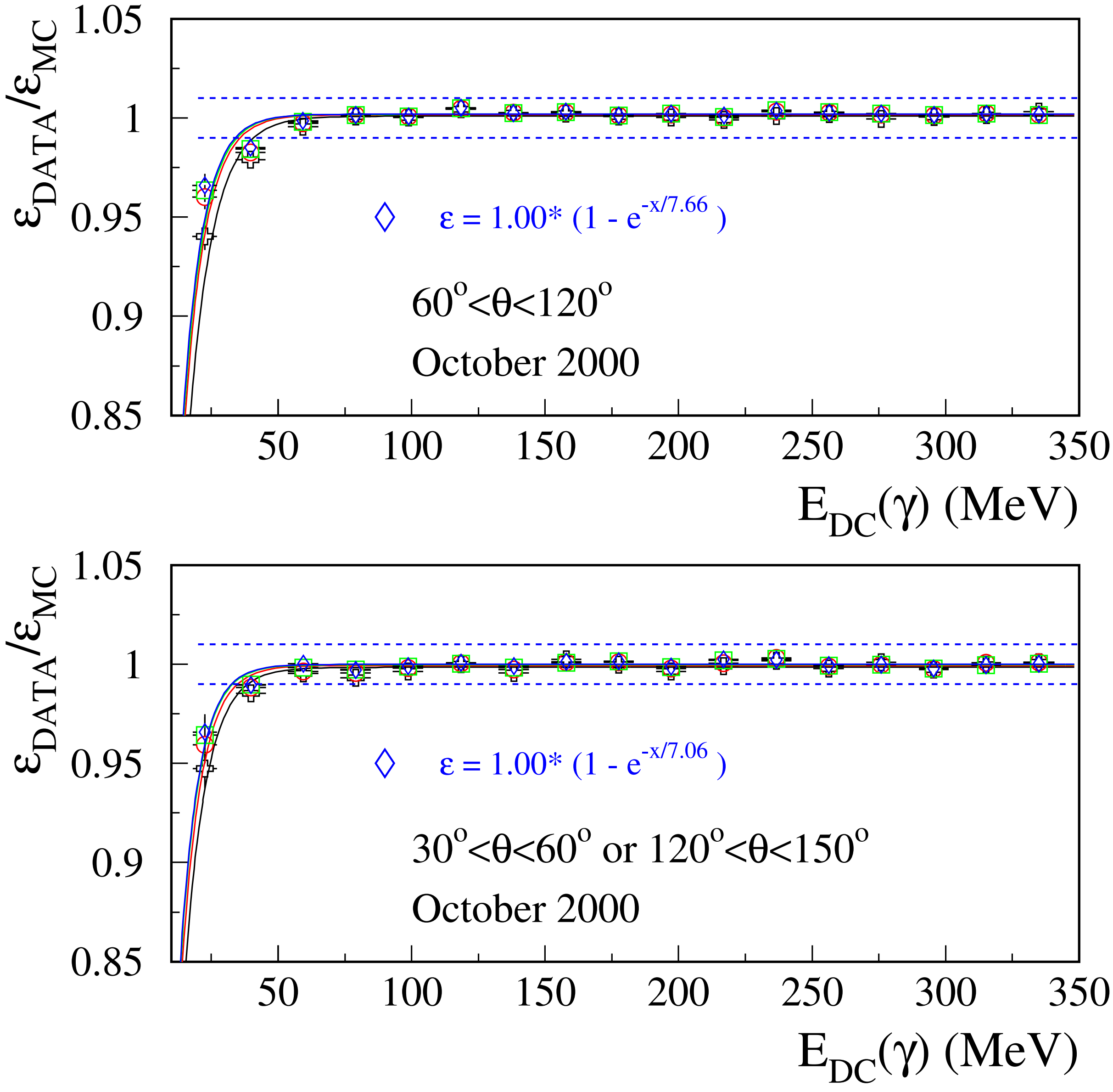

Figure 23: Ratio of data and Monte Carlo photon detection efficiencies as a function of the expected photon energy, in two 60°-slices of the photon polar angle. The different symbols correspond to the candidate-matching definitions $\cos_{\rm min} = 0.6, 0.7, 0.8, 0.9$. The dashed lines represent a ±1%-band.

This has been done by applying the ratio of efficiencies (Fig. 23) as a direct correction to the Monte Carlo simulation: for each photon entering the calorimeter for which an associated cluster is reconstructed, the cluster is “switched off” according to this ratio, thus shifting the prompt cluster multiplicity towards lower values (Table 2).

The relative variations for the prompt cluster acceptances are: a factor -0.2% for $\varepsilon_{\mathrm{N}\geq 3}$, and a factor -0.7% for the $\varepsilon_{\mathrm{N}\geq 4}$ value: as expected, the analysis with the looser inclusive cut is more robust.[2)]

N_{prompt}	MC Acceptance (%)	MC Acceptance corrected (%)
2	8.46 ± 0.04	8.59 ± 0.04
3	33.42 ± 0.07	33.67 ± 0.07
≥ 3	90.22 ± 0.05	90.05 ± 0.05
≥ 4	56.80 ± 0.08	56.39 ± 0.08

Table 2: Acceptance of the cuts on the minimum number of neutral prompt clusters, estimated by Monte Carlo. The results obtained using not corrected and data-corrected Monte Carlo energy thresholds are compared.

In the following, the $N \geq 3$ cut will be used, since it guarantees a lower systematic error. The efficiency is taken from the corrected Monte Carlo and the correction is assumed as systematic error:

$$\boxed{\varepsilon^{00}_{\mathrm{sele}} = (90.05 \pm 0.05_{\mathrm{stat}} \pm 0.17_{\mathrm{syst}})\,\%.} \tag{6}$$

5 Trigger and t_0 efficiencies for $K_S \to \pi^0\pi^0$ events

The efficiencies that at least a golden-t_0 cluster is found for the selected events, and that the event is triggered, are discussed as conditional probabilities.

The t_0 efficiency, namely the probability that in a $K_S \to \pi^0\pi^0$ selected event, at least one K_S cluster satisfies the golden-t_0, is estimated directly from data using a $K_L \to \pi^+\pi^-\pi^0$ sample [11], which is independent from the global-t_0 estimate. In order to avoid any bias due to the trigger conditions, these are required to be satisfied using the K_L clusters only. Then, the $K_S \to \pi^0\pi^0$ selection is applied: on a sample of 2 700 events with three or more prompt clusters, the golden-t_0 condition is always satisfied. This corresponds to an efficiency better than 99.9% (90% confidence level).

In order to estimate the trigger efficiency in a $K_S \to \pi^0\pi^0$ selected event, *given the* K_{crash}*-tag*, direct use has been done of a selected data sample of $K_S \to \pi^0\pi^0$ events. The method [12] aims first at separating the reconstructed clusters into K_S-derived and K_L-derived categories; then, starting from the recostructed clusters, the trigger sectors fired by K_S or K_L are identified. The distribution of trigger sectors fired by the K_S (K_L) are calculated requiring that the K_L (K_S) alone satisfies the trigger conditions. Finally, the probability to trigger the event is:

$$\varepsilon_{\mathrm{trig}}\left(K_S \to \pi^0\pi^0\right) = 1 - \varepsilon_{\mathrm{L}}(1) \times \varepsilon_{\mathrm{S}}(0) = \varepsilon_{\mathrm{L}}(\geq 2) + \varepsilon_{\mathrm{L}}(1) \times \varepsilon_{\mathrm{S}}(\geq 1) \tag{7}$$

where $\varepsilon_{\mathrm{L,S}}(n)$ is the probability, calculated for the $K_{L,S}$ to fire n trigger sectors. It has indeed to be underlined that **in a K_{crash}-tagged event the K_L always produces at least one fired trigger sector (on the barrel).**

[2)] Since $\Delta N_{\geq 3}/N_{\geq 3} = N_{=3}/N_{\geq 3} \times 3P$ and $\Delta N_{\geq 4}/N_{\geq 4} = N_{=4}/N_{\geq 4} \times 4P$, where P is the average “switching off” probability.

In a $K_{\rm crash}$-tagged $K_S \to \pi^0\pi^0$-selected event, K_S and K_L clusters can be separated just by using the cluster time. For each cluster in the event (other than the $K_{\rm crash}$-identified cluster), the difference in time with respect to the $K_{\rm crash}$-cluster is calculated. As shown in Fig. 24, two structures are cleanly separated: the distribution below -15 ns is practically independent on the $K_{\rm crash}$ energy cut, and is attributed to the K_S. The distribution above -15 ns is due to residual cluster-fragments of the K_L (either close split fragments, or flying photons), and is depressed as the $K_{\rm crash}$ energy increases.

Using a $K_{\rm crash}$-energy cut of 100 MeV, both the probability to have only one trigger sectors fired by the K_L, and the one to have no sectors due to the K_S are calculated:

$$
\begin{aligned}
\varepsilon_{\rm L}\,(1) &= (58.2 \pm 0.3_{\rm stat} \pm 1.5_{\rm syst})\,\% \\
\varepsilon_{\rm S}\,(0) &= (0.33 \pm 0.004_{\rm stat} \pm 0.03_{\rm syst})\,\% \text{ with } N_{\rm prompt} \geq 3 \\
\varepsilon_{\rm S}\,(0) &= (0.056 \pm 0.006_{\rm stat} \pm 0.008_{\rm syst})\,\% \text{ with } N_{\rm prompt} \geq 4
\end{aligned}
$$

From these, using Eq. (7), the results for the trigger efficiency are:

$$\boxed{\varepsilon_{\rm trig}\,(K_S \to \pi^0\pi^0) = (99.78 \pm 0.003_{\rm stat} \pm 0.04_{\rm syst})\,\% \;\; \text{Selection: } N_{\rm prompt} \geq 3} \tag{8a}$$

$$\varepsilon_{\rm trig}\left(K_S \to \pi^0\pi^0\right) = (99.95 \pm 0.004_{\rm stat} \pm 0.02_{\rm syst})\,\% \text{ Selection: } N_{\rm prompt} \geq 4 \tag{8b}$$

The systematic error arises from the presence of sectors fired both by K_L and K_S. The quoted systematic error is the maximum variation in the probabilities obtained by assigning all of the “overlaps” either to the K_S or to the K_L sectors. Note that, since the K_S zero-probabilities $\varepsilon_{\rm S}\,(0)$ are low, the overlaps have a sizable *absolute* effect mainly on the K_L efficiency.

The effectiveness of the separation between K_S and K_L trigger sectors has been probed by varying the $K_{\rm crash}$-energy cut, between 100 MeV and 350 MeV. The probability to produce the trigger by itself has been calculated both for K_L and for K_S. The K_L-trigger probability significantly increases with the $K_{\rm crash}$-energy cut (Fig. 25), while – as expected – the K_S-trigger probability is stable within the total estimate error (Fig. 26).

6 Background in $K_S \to \pi^0\pi^0$ events

In this section the methods applied to estimate the backgrond level in the sample of events selected as $K_S \to \pi^0\pi^0$ are discussed. Two type of background are distinguished: $K_S \to \pi^+\pi^-$ events, in which three or more prompt cluster are found, due to the splitting and accidentals contributions; other background events, either machine background or cosmic-ray events, or events in which $\phi \not\to K_S K_L$. The contribution of $K_S \to \pi^+\pi^-$ events actually has been already estimated in the general discussion of the splitting and accidentals (Sect. 3). A study has been also performed using a sample of Monte Carlo $K_S \to \pi^+\pi^-$ events, equivalent to an integrated luminosity of ~ 3 pb^{-1}. The observed background level (three or more prompt clusters) is well below 10^{-3}. However, the effectiveness of those estimates can be probed directly using data, by two different methods.

1. In order to evaluate the background content of the β^* distribution, two different regions of the spectrum are defined: the “$\pi^0\pi^0$-peak” and the “$\pi^+\pi^-$-peak” (Fig. 27). The β^* distributions of $K_S \to \pi^+\pi^-$ and $K_S \to \pi^0\pi^0$ have well separated peaks, while the other background events are expected to be uniformly distributed. Hence, the fractional contribution of background events should be different: lower in the $\pi^0\pi^0$-peak, significantly

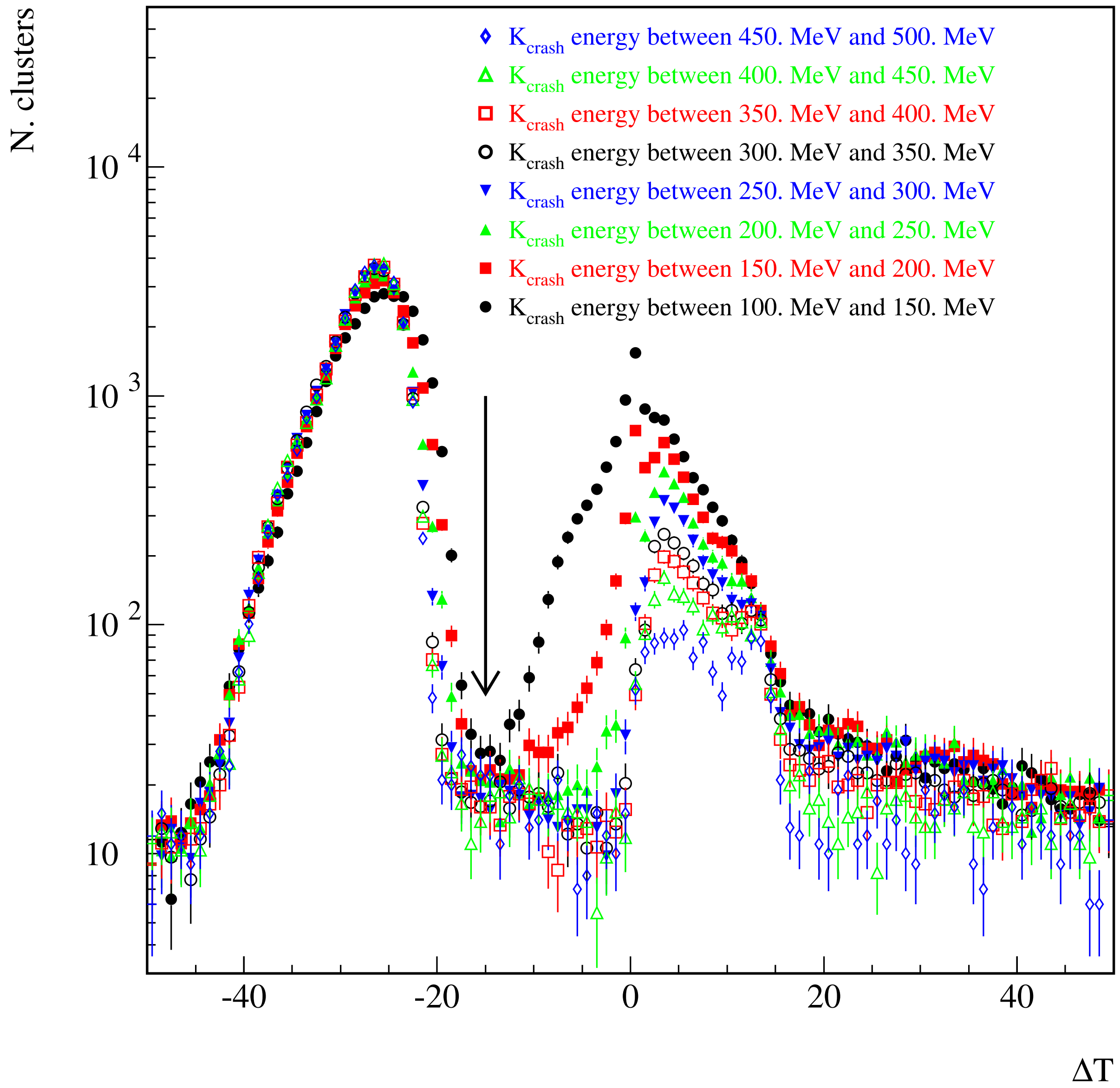

Figure 24: $K_{\rm crash}$-tagged events, identified as $K_S \rightarrow \pi^0\pi^0$. Distribution of the difference in time of each cluster with respect to the $K_{\rm crash}$-cluster. In the plot there is one entry for each cluster in the event with energy above 20 MeV ($K_{\rm crash}$-cluster excepted). As the $K_{\rm crash}$energy increases, the distributions for time differences below -15 ns (K_S-cluster-region) is invariant, while the remaining distribution (K_L-cluster-fragments region) become more and more depopulated.

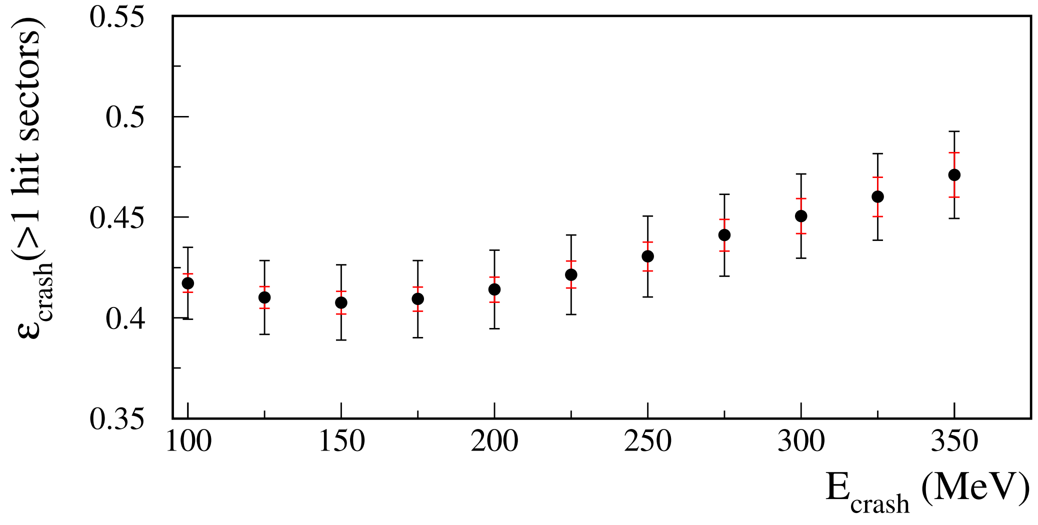

Figure 25: Efficiency for the K_L to satisfy the trigger conditions by itself, in K_{crash} events, as function of the energy cut used in the K_{crash}-tagging. The efficiency is estimated using a $K_S \to \pi^0\pi^0$ control sample. The shorter bar represents the statistical error, while the longer one is the systematic uncertainty.

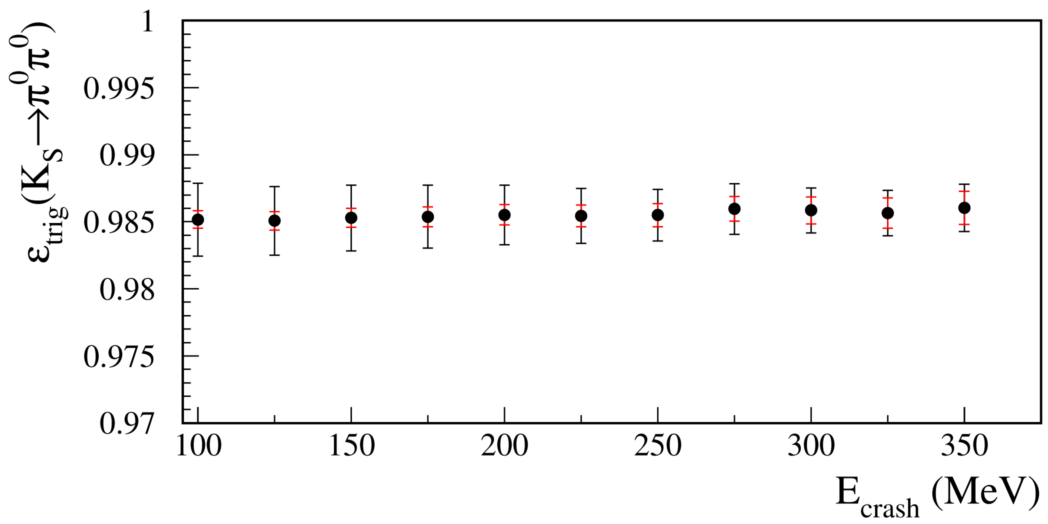

Figure 26: Probability for the K_S to satisfy the trigger conditions by itself, in $K_S \to \pi^0\pi^0$ events. The probability is estimated using events tagged by the K_{crash}-algorithm, as a function of the K_{crash}energy cut; the result is stable within the errors: the shorter bar represents the statistical error, while the longer one is the systematic uncertainty.

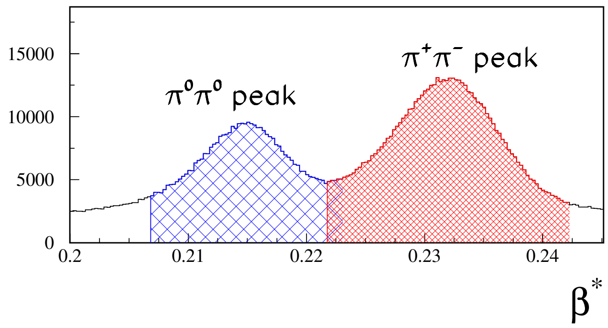

Figure 27: Definition of the two β^* regions used in the background evaluation.

higher in the $\pi^+\pi^-$-peak, where the tail of the distribution for $\pi^0\pi^0$ events is superimposed to the $\pi^+\pi^-$ peaking distribution and to the flat background contribution. In the two β^* regions, the ratios

$$R_{1,2} = \frac{N_3^{\rm obs}\,(\text{region 1,2})}{N_4^{\rm obs}\,(\text{region 1,2})}$$

are computed, being independent from the number of events. Since the $K_S \to \pi^+\pi^-$ content in four-prompt events is expected to be significantly lower than in the three-prompts, a difference between R_1 and R_2 signals a contamination of $K_S \to \pi^+\pi^-$ events in the three-prompt sample. Moreover, other background events are expected to be suppressed at higher $K_{\rm crash}$ energies, more than K_SK_L events. Therefore, the ratios are evaluated as a function of the $K_{\rm crash}$ energy cut.

In Fig. 28 (left) the ratios are compared with the value obtained using the entire β^* window. The ratios evaluated in the $\pi^0\pi^0$-peak are compatible within the errors with the

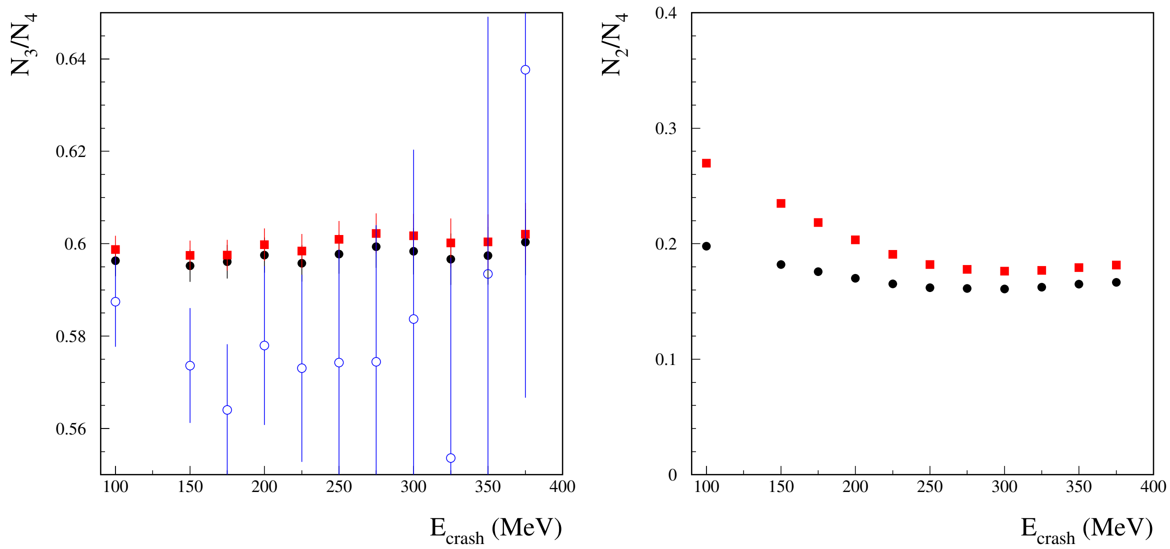

Figure 28: The ratio of events with three (two) and four prompt clusters are shown in the left (right) plot, as a function of the $K_{\rm crash}$ energy cut, for different β^* regions: $\pi^0\pi^0$-peak (solid circles), $\pi^+\pi^-$-peak (open circles), and the entire β^*-window (solid squares).

value for the entire β^*-window, without any significant dependence on the $K_{\rm crash}$ energy. The values for the $\pi^+\pi^-$-peak are different, up to 2%. However, their weight in the total contamination is as low as 10% since only the tail enters the selection. This indicates that the background level in the photon counting does not exceed 2×10^{-3}.

As a cross-check for this method, the two neutral-prompt cluster sample, not used in the analysis, is also studied. A relevant contamination is expected in these events. This is indeed the case, as proved by the ratio

$$R_{1,2} = \frac{N_2^{\mathrm{obs}}\,(\mathrm{region}\ 1{,}2)}{N_4^{\mathrm{obs}}\,(\mathrm{region}\ 1{,}2)}$$

shown in Fig. 28 (right): by increasing the K_{crash} energy, the ratio calculated in the $\pi^+\pi^-$-peak decreases and gets similar to the value of the $\pi^0\pi^0$-window. This actually means that the initial discrepancy is due to background and is lowered by applying a tighter cut.

2. The contamination of $K_S \to \pi^+\pi^-$ events has been also estimated by looking at the multiplicity of tracks coming from the interaction point, as a function of the number of prompt clusters (see table 3).

Topology	MC	Data
% of 3-prompt evts with 1 track	2.90 ± 0.05	3.56 ± 0.03
% of 3-prompt evts with 2 tracks	1.49 ± 0.03	1.50 ± 0.02
% of 4-prompt evts with 1 track	0.069 ± 0.005	0.239 ± 0.006
% of 4-prompt evts with 2 tracks	0.016 ± 0.003	0.057 ± 0.003
% of $\geq$ 3-prompt evts with $\geq$ 1 tracks	1.69 ± 0.02	2.07 ± 0.01

Table 3: Multiplicity of tracks originating from the interaction point, as a function of the number of prompt clusters in the event, for data and Monte Carlo $K_S \to \pi^0\pi^0$ events.

There are three possible sources of tracks: $K_S \to \pi^+\pi^-$ events contaminating the sample, spurious tracks from machine background accidentally overlapped to $K_S \to \pi^0\pi^0$ events, and $K_S \to \pi^0\pi^0$ events with a photon conversion in the material traversed before entering the Calorimeter or with one $\pi^0 \to e^+e^-\gamma$ (Dalitz) decay.

This last category, which is also simulated in the Monte Carlo, dominates the track multiplicity in events with three prompt clusters: in particular, there is a good agreement between the fraction of events with two tracks coming from the IP observed in data and Monte Carlo (second row in table 3); on the contrary, the small excess (first row) of 1-track events in data could be due either to machine background, or to a different treatment of photon conversion in the traversed material.

The presence of spurious tracks dominates the multiplicity in four-prompt events in data. The random overlap of tracks external to the main event occur in a correlated fashion. This is indeed suggested by observing that the probability of having a two-track event (fourth row) is much greater than the square of that of having a one-track event (third row).

Finally, the background due to $K_S \to \pi^+\pi^-$ in the selected events can be estimated assuming a probability of having one or more spurious track equal to $(0.296 \pm 0.007)\%$ (third row + fourth row) and correcting accordingly the Monte Carlo (fifth row). This gives a contamination of $(0.084 \pm 0.002)\%$.

7 Selection of $K_S \to \pi^+\pi^-$ events

The selection of $K_S \to \pi^+\pi^-$ events is based on the identification of both the K_S pion tracks, mainly obtained by applying topological requirements with very loose kinematical cuts. Since the possible background due to charged modes other than $K_S \to \pi^+\pi^-(\gamma)$ (semileptonic K_S decays and $K_S \to \pi^0\pi^0$ decays in which a π^0 undergoes a Dalitz pair decay, $\phi \to K^+K^-$ decays) amounts to few 10^{-3}, these cuts are sufficient to select a clean sample of $K_S \to \pi^+\pi^-$ decays.

In a K_{crash}-tagged event, all of the tracks starting close to the drift chamber wall are considered: the first hit is required to be within the cylindrical volume:

$$\sqrt{X^2_{\text{first}} + Y^2_{\text{first}}} \leq 40 \text{ cm AND } |Z_{\text{first}}| \leq 40 \text{ cm} \tag{9}$$

This means that the track has to start by one of the five innermost layers of the chamber. An acceptance cut is also imposed on the polar angle θ_{trk} of the momentum, which is required to be in the range:

$$30^\circ \leq \theta_{\text{trk}} \leq 150^\circ \tag{10}$$

The tuning of these preliminary cuts has been performed in order to simplify the implementation of the correction due to the track-reconstruction efficiency. Using the cuts listed above, this correction reduces to a constant independent on the pion track momentum, as described in Sect. 8.

All of the considered tracks are then extrapolated at the point of closest approach to the origin (PCA). The beam-transverse ($\rho_{\text{PCA}} = \sqrt{X^2_{\text{PCA}} + Y^2_{\text{PCA}}}$) and beam-longitudinal (Z_{PCA}) distances of closest approach are then calculated (Fig. 29). The applied cut

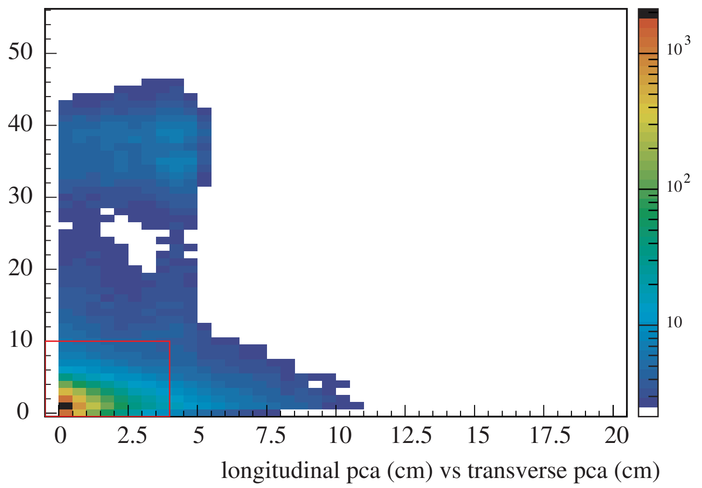

Figure 29: Distribution of the longitudinal (z) vs. transverse (ρ) distances of the point of closest approach to the origin, in K_{crash}-tagged events in Summer 2000 data. To select $K_S \to \pi^+\pi^-$ events, tracks are required to come from the IP, in order to reject the background due to particles hitting the quadrupole flanges (at $|z| \simeq 40$ cm). A rectangular cut is applied in the longitudinal vs transverse position of the minimum approach of the track to the IP.

$$\rho_{\text{PCA}} \leq 4 \text{ cm AND } |Z_{\text{PCA}}| \leq 10 \text{ cm}$$

aims at rejecting the tracks of machine-background events, which mostly originate from the quadrupoles. These tracks have small values of ρ_{PCA}, but are away in $|Z_{\mathrm{PCA}}|$ (by ~ 40 cm).

In addition, in order to select events with higher probability of having a K_S golden-T0 cluster [Eq. (4)], the following cuts are applied. In order to reject spiralizing tracks, for which the Monte Carlo simulation is not reliable, the tracks re-entering the internal DC wall at some point along the extrapolated path are rejected. A cut is imposed on the transverse position $\rho_{\mathrm{extrap}} = \sqrt{x^2_{\mathrm{extrap}} + y^2_{\mathrm{extrap}}}$ of the track-impact point. To summarize, the track acceptance cuts are listed below:

$$\text{No forward impact on the DC internal wall} \tag{11a}$$

$$\rho_{\mathrm{extrap}} \geq 60 \text{ cm} \tag{11b}$$

A loose cut on the momentum P_{trk} of the selected tracks is finally applied, in order to reject the small background due to $\phi \to K^+K^-$ decays and residual machine-background events (Fig. 30):

$$120 \text{ MeV} \leq P_{\mathrm{trk}} \leq 300 \text{ MeV} \tag{12}$$

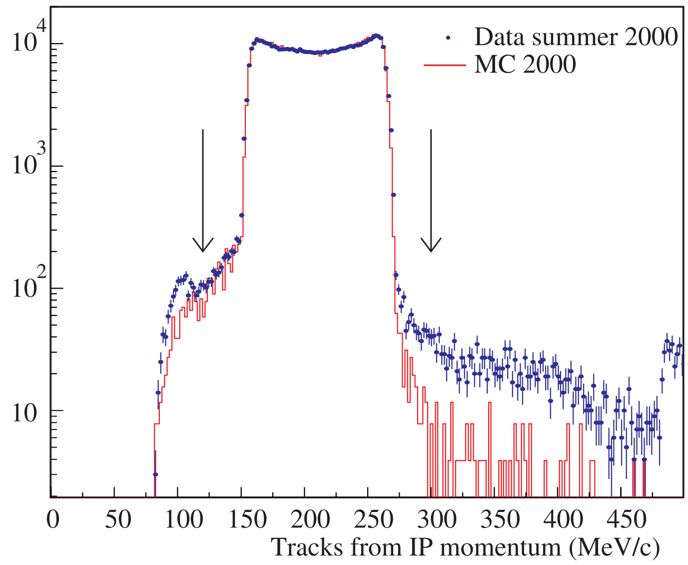

Figure 30: Distribution of the track momentum, for K_{crash}-tagged events with a pair of selected tracks (circles) and for $K_S \to \pi^+\pi^-$ Monte Carlo events (solid line). The excess of population visible around 100 MeV is due to $K^\pm$ tracks, while the high-momentum region is dominated by residual background of tracks due to the machine.

At least a pair of tracks of opposite curvatures, completely disconnected one from each other, satisfying all of the previous cuts, is required.

The selection efficiency is defined as the probability that, *given the K_{crash}-tag*, at least two tracks of opposite charge coming from the interaction point (IP) are selected, at least a golden-t_0 cluster is found, and the event is triggered.

The track-selection efficiency has been estimated in two steps (Sect. 8). First the track reconstruction efficiency is extracted directly from data samples of $K_S \to \pi^+\pi^-$ with a K_{crash}-tag, as a function of the track transverse momentum and polar angle; then, the efficiency profiles are used to correct the Monte Carlo simulation and the data-tuned Monte Carlo is used to calculate the efficiency of the track-selection.

The t_0 and trigger has been estimated using two methods: directly from data using $K_L \to \pi^+\pi^-\pi^0$-tagged data samples, and tuning the Monte Carlo simulation with data-extracted efficiencies (Sect. 10).

8 Tracking efficiency

The efficiency to reconstruct a track is extracted directly from subsamples of $K_S \to \pi^+\pi^-$ events, using the K_{crash}-tag derived information.

Given a K_{crash}-tagged event, the $K_S \to \pi^+\pi^-$ decay is selected with low background by tightly identifying only one pion track: the same acceptance cuts described above have been used, with a harder momentum cut ($150 \leq p \leq 260$ MeV/c). The transverse momentum P_{T} and polar angle θ of the other track are then estimated by kinematically closing the event, using the K_S-momentum $\mathbf{P}_{\mathrm{S}}$ derived by the K_{crash} cluster direction:

$$\mathbf{p}_{\mathrm{other}} = \mathbf{P}_{\mathrm{S}} - \mathbf{p}_1 = \mathbf{P}_\phi - \mathbf{P}_L - \mathbf{p}_1$$

In a K_{crash}-event, the K_L-momentum can in fact be calculated by using the K_L-clusters position, and the ϕ boost (β and γ) and $\sqrt{s}$ estimated run-by-run from Bhabha events [5]. The other track is *matched* if another track with curvature opposite to the previous one is selected.

To check the validity of this method, the distributions of the components of the missing momentum $\mathbf{\Delta P} = \mathbf{p}_1 + \mathbf{p}_{\mathrm{other}}^{\mathrm{meas}} - (\mathbf{P}_\phi - \mathbf{P}_L)$ for data and Monte Carlo simulated events are compared in Fig. 31 (when the other track is found); both distribution are normalized to the same number of events. The agreement is good, showing a momentum resolution of $\approx$2 MeV/c.

Finally, the track-reconstruction efficiency is calculated in bins 10 MeV $\otimes$ 1° wide in the plane $P_{\mathrm{T}} \otimes \theta$. The efficiency is defined as

$$\varepsilon_{\mathrm{trk}}(\theta, p_{\mathrm{t}}) = \frac{\#\text{ of evts. in a } P_{\mathrm{T}} \otimes \theta\text{-bin with a } \textit{matched} \text{ track}}{\text{Total } \#\text{ of evts. in a } P_{\mathrm{T}} \otimes \theta\text{-bin}}$$

The estimated efficiency is shown in Fig. 32:

- The tracking efficiency shows a good stability in the different running periods (the first runs of year 2001 data taking are also shown);
- The tracking efficiency exceeds 95% in the region allowed by the acceptance cuts described above.

The tracking efficiency has been studied also on Monte Carlo $K_S \to \pi^+\pi^-$ events. The value of the plateau of the tracking efficiency of data and Monte Carlo is shown in Fig. 33 as a function of the cut on the first hit of Eq. (9). The tracking efficiency on data is in fact sensitive to this cut, due to the presence of spurious hits in the very first layers of the chamber: those additional hits reduce the fraction of good hits associated to the track.

Since spurious hits are not simulated in the Monte Carlo, the tracking efficiency in this case is higher. The effect on data can be reduced making the cut looser, thus optimizing the data/Monte Carlo ratio. With the choice of Eq. (9) the ratio is about 99%, as shown in Fig. 34 as a function of the transverse momentum P_{T} and the polar angle θ of the emitted tracks.

In Fig. 35, the data/MC ratio is also shown as a function of the θ (P_{T}) variable only, for accepted tracks. The behaviour is flat over the accepted range.

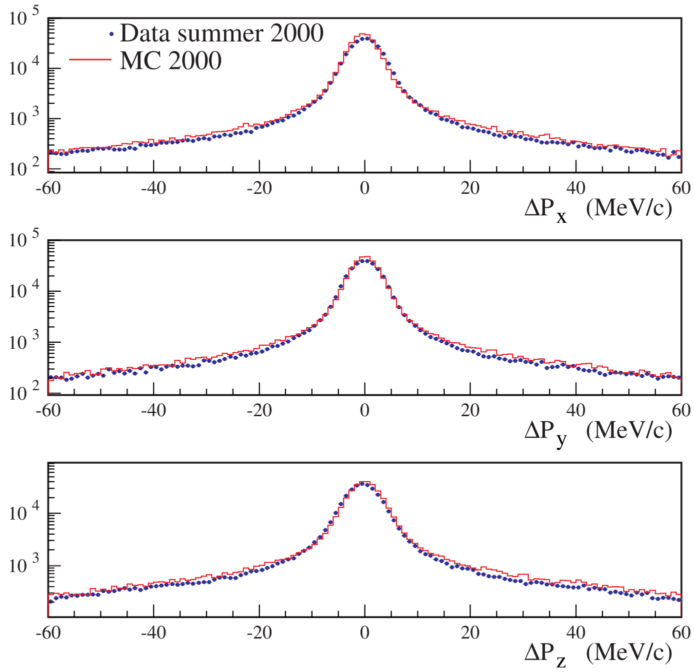

Figure 31: Resolution in the missing momentum for $K_S \to \pi^+\pi^-$ events, where the K_S momentum has been estimated using the K_{crash} cluster information and the ϕ 4-momentum. Distributions of x, y, and z components are plotted for August 2000 data taking and $K_S \to \pi^+\pi^-$ Monte Carlo, normalized to the same number of events.

9 Acceptance calculation for $K_S \to \pi^+\pi^-$ events

The selection efficiency is estimated directly using the Monte Carlo simulation.

Since the data/MC ratio of tracking efficiencies is constant over the accepted range, we use an average value C_{track} over the P_{T}–θ plane to correct the Monte Carlo tracking efficiency (per single track), according to the equation:

$$\varepsilon^{\pm}_{\text{sele}} = \frac{\varepsilon^{\pm}_{\text{seleMC}}}{C^2_{\text{track}}} \,, \tag{13}$$

where $\varepsilon^{\pm}_{\text{seleMC}} = (58.9 \pm 0.1_{\text{stat}})\,\%$, with a statistical error due to the limited Monte Carlo statistics.

C_{track} is the result of a fit to a constant performed in the region defined by the acceptance cuts of Eqs. (10) and (12) (that delimited by the solid lines in Fig. 34). Slightly different values for the ratio are obtained for different subsamples, due to different levels of background. The value used to correct the $K_S \to \pi^+\pi^-$ counts is the weighted average over the samples, with a systematic error estimated as the maximum spread. The result is:

$$C_{\text{track}} = \left\langle \frac{\varepsilon_{\text{track}}\,(\text{Data})}{\varepsilon_{\text{track}}\,(\text{MC})} \right\rangle = (99.0 \pm 0.1)\,\%$$

9.1 Acceptance for $K_S \to \pi^+\pi^-(\gamma)$ events

The Monte Carlo simulation used for the evaluation of the selection efficiency does not take into account the presence of a soft photon in the final state. Even though the cut on the track momenta is very loose, the requirement to have *both* tracks entering the

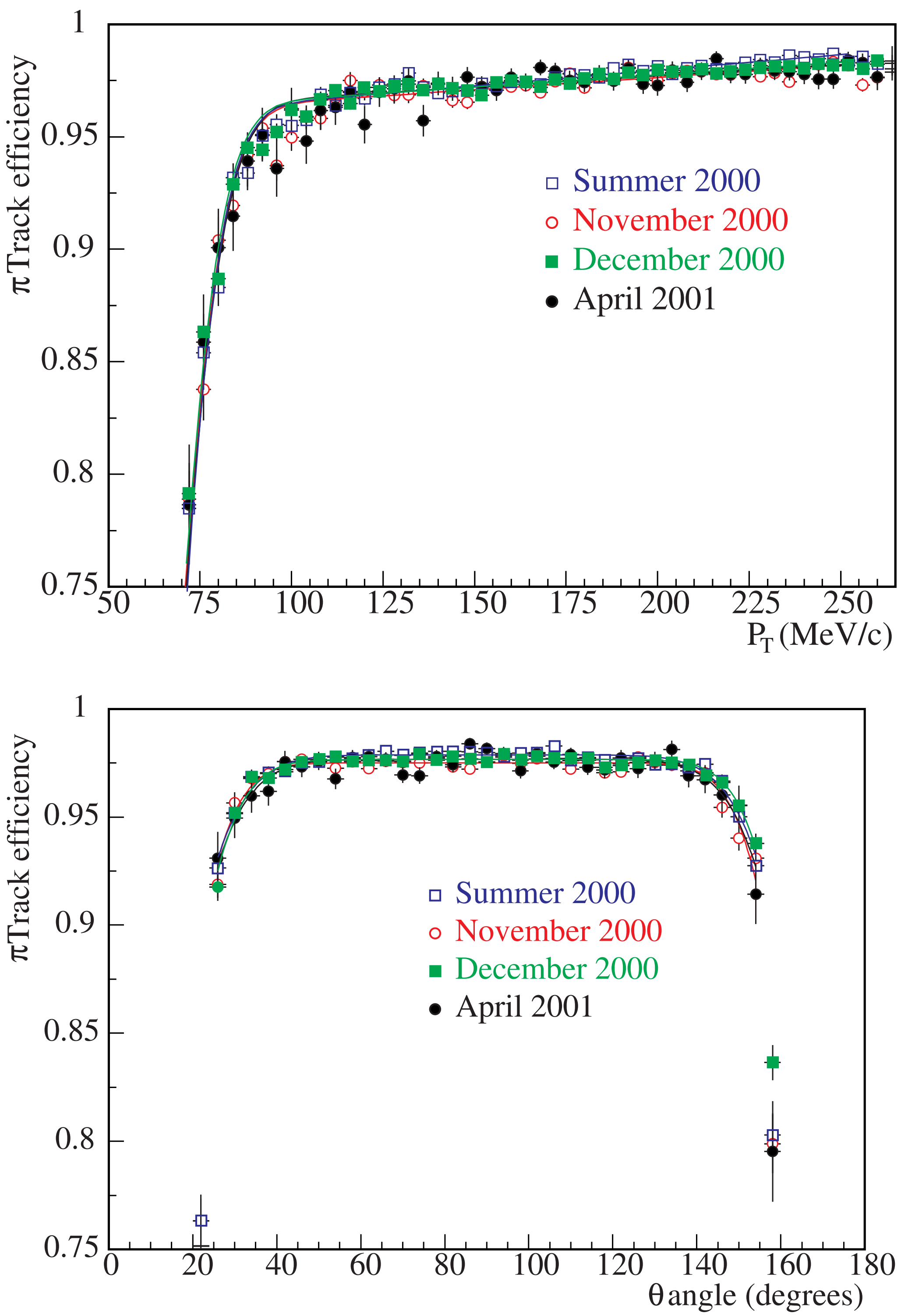

Figure 32: Tracking efficiency vs. transverse momentum (top) and polar angle (bottom) for four different data samples.

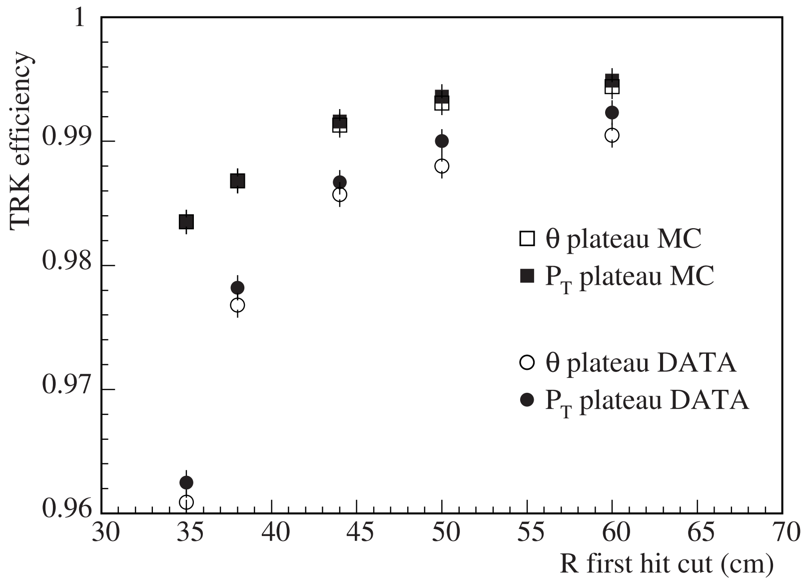

Figure 33: Tracking efficiency: the efficiency plateau value is shown as a function of the cut on the first hit in the drift chamber ($R_{\rm first}$), for summer 2000 data (circles) and for Monte Carlo (squares). Both the P_T (full symbols) and θ (open symbols) distributions are shown: hardening the $R_{\rm first}$ cut the efficiency of data with respect to the Monte Carlo get worse because of the reduced cell efficiency of the inner layers of the chamber (noisy channels).

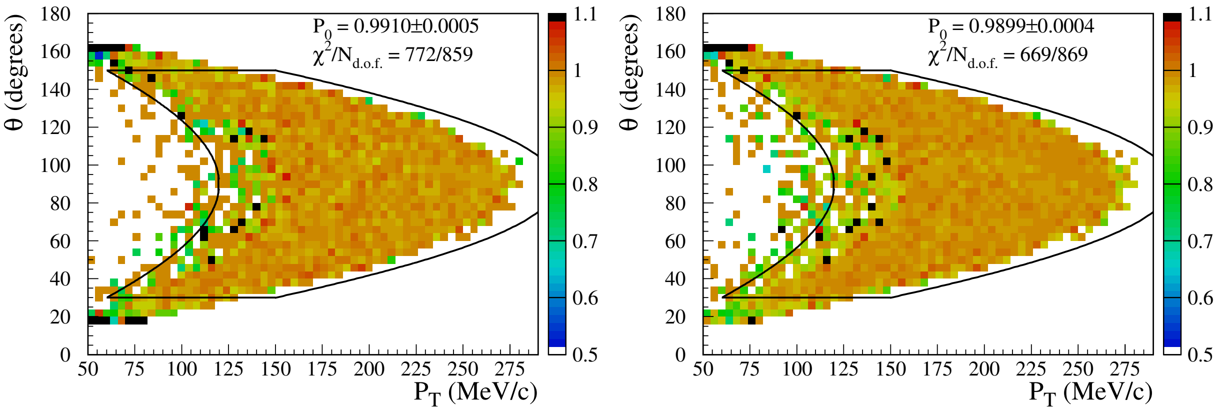

Figure 34: Tracking efficiency: Data/Monte Carlo ratio vs. transverse momentum and polar angle for two different periods of data taking: November 2000 (left) and December 2000 (right). The result of the fit to a constant over the accepted region (delimited by the solid lines) is shown.

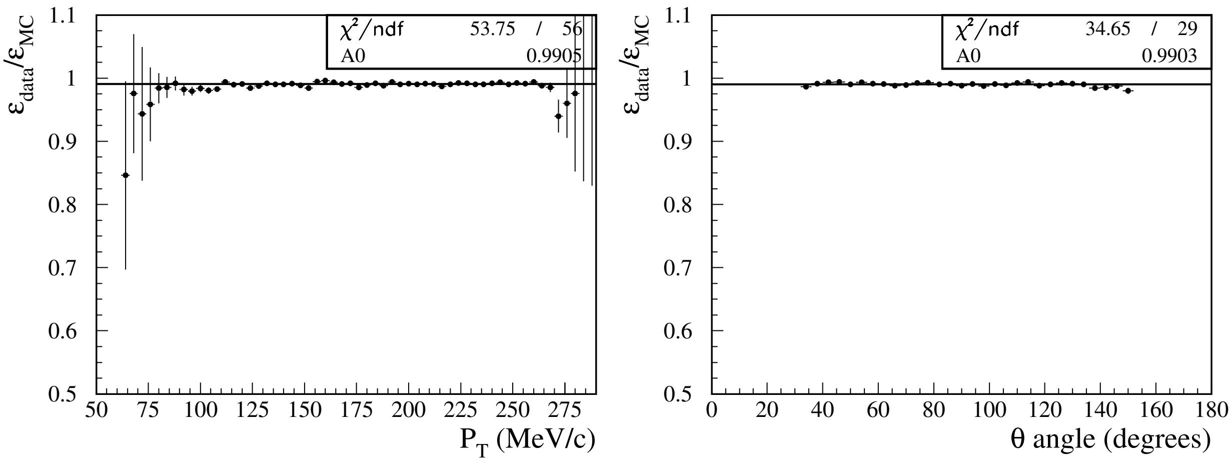

Figure 35: Tracking efficiency: Data/Monte Carlo ratio as a function of the transverse momentum (left) and polar angle (right) for December 2000 data.

calorimeter without spiralling introduces a bias on the acceptance as a function of the energy E^*_γ of the radiated photon in the K_S rest frame. A prescription has then to be applied on the radiated photon: the measurement of the ratio $\Gamma(K_S \to \pi^+\pi^-)/\Gamma(K_S \to \pi^0\pi^0)$ can be performed either in a fully inclusive way, or with a fixed cutoff for E^*_γ.

Then the efficiency $\varepsilon_{\pi\pi\gamma}(E)$ has been evaluated as a function of E^*_γ, by using a Monte Carlo sample of $K_S \to \pi^+\pi^-(\gamma)$ events, generated with $E^*_\gamma > 20$ MeV, together with the above sample of $K_S \to \pi^+\pi^-$ MC events. It is shown in Fig. 36 (solid circles). A linear fit has been performed on this distribution in order to extrapolate the efficiency below 20 MeV.

The approach of reference[13] has been followed to estimate the convolution of this selection efficiency with the photon spectrum. The infrared (IR) divergence of the amplitude $\mathcal{A}$ for $K_S \to \pi^+\pi^-(\gamma)$ can be expressed with an exponential, when all orders of the expansion in α (fine structure constant) are summed:

$$\mathcal{A}(\alpha) = e^{\alpha B(\lambda)}\overline{\mathcal{A}}(\alpha)$$

where an IR regulator λ, for example a fictitious photon mass m_γ, is introduced; $B(\lambda)$ is an IR-divergent function, and $\overline{\mathcal{A}}$ is an IR-finite amplitude, which contains the structure dependent electromagnetic effects. The measured decay width $\hat{\Gamma}_\pm$ depends on the way in which soft photons are treated in data analysis:

$$\hat{\Gamma}_\pm\left(E^*_\gamma < \omega\right) = \frac{p_\pm}{4\pi M_K^2}\left|\overline{\mathcal{A}}_\pm\right|^2 \hat{G}_\pm(\omega)$$

where ω is the maximum energy for detected real photons, $p_\pm$ is the pion momentum in the K_S rest frame, and $\hat{G}_\pm$ is factor associated with the combined effect of virtual (in $K_S \to \pi^+\pi^-$) and real (in $K_S \to \pi^+\pi^-(\gamma)$) photons:

$$\begin{aligned} G_\pm(\omega) &= \underbrace{1 + 2\alpha\Re(m_\gamma)}_{\text{from } K_S\to\pi^+\pi^-} + \underbrace{I_\pm(m_\gamma,\omega)}_{\text{from } K_S\to\pi^+\pi^-(\gamma)} + \mathcal{O}\left(\alpha^2\right) \\ I_\pm(m_\gamma,\omega) &= \int_{E^*_\gamma<\omega} \frac{\mathrm{d}^3 q}{(2\pi)^3\, 2E^*_\gamma}\sum_{\text{pol}}\left|\frac{\mathcal{A}^{\text{IB}}_{\pm\gamma}}{\mathcal{A}_\pm}\right|^2 \end{aligned}$$

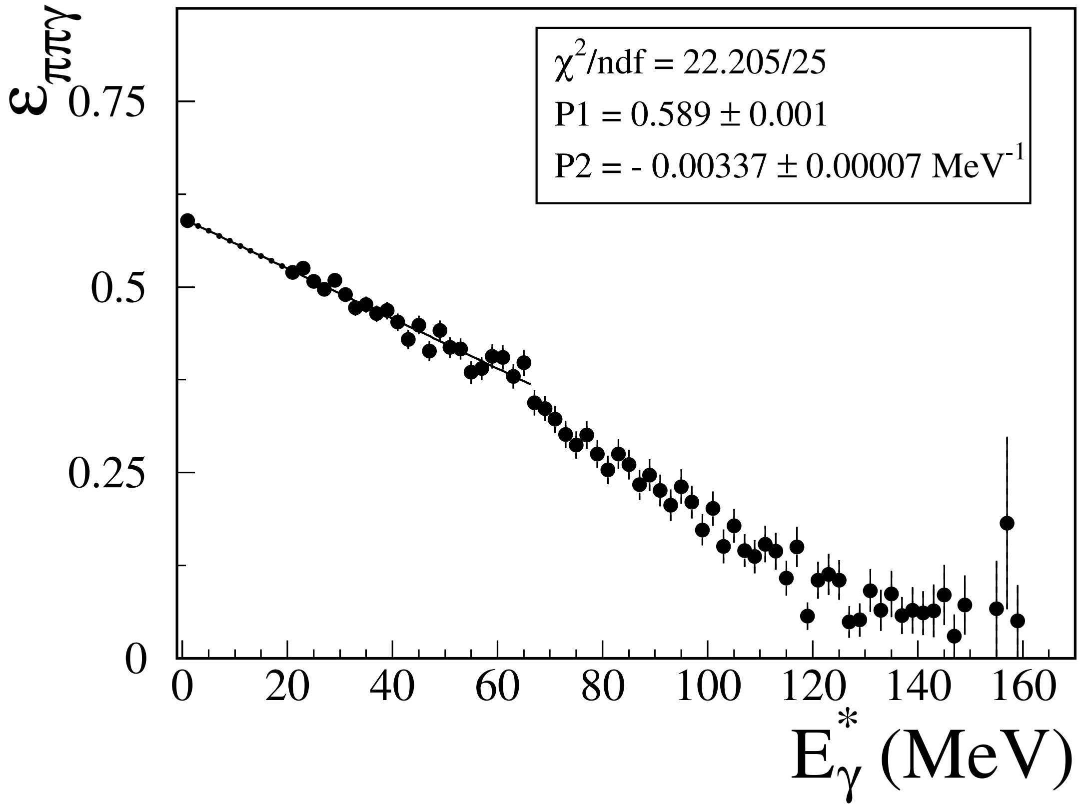

Figure 36: The selection efficiency is shown as a function of the energy of the radiated photon in the K_S rest frame (solid circles), for $K_S \to \pi^+\pi^-(\gamma)$ MC events, above 20 MeV, and $K_S \to \pi^+\pi^-$ MC events at zero. The result from a linear fit performed for energies below 60 MeV is superimposed:

Both contributions are IR-divergent (for $m_\gamma \to 0$), while their sum is finite. In this analysis no explicit cut is applied on the photon energy, so $\omega = (M_K^2 - M_\pi^2)/(2M_K) \simeq 170$ MeV. However, the selection efficiency does depend on E^*_γ, as shown in Fig. 36, and should be used in the integral over the $K_S \to \pi^+\pi^-(\gamma)$ phase space $I_\pm$. The correct expression for $\hat{G}$ should be:

$$\begin{aligned}
\hat{G}_\pm(\omega) &= \underbrace{\varepsilon_{\text{sele}}(0)\left[1 + 2\alpha\Re(m_\gamma)\right]}_{\text{from } K_S\to\pi^+\pi^-} + \underbrace{\hat{I}_\pm(m_\gamma,\omega)}_{\text{from } K_S\to\pi^+\pi^-(\gamma)} + \mathcal{O}\left(\alpha^2\right) \\
\hat{I}_\pm(m_\gamma,\omega) &= \int_{E^*_\gamma<\omega} \frac{\mathrm{d}^3q}{(2\pi)^3\,2E^*_\gamma}\varepsilon_{\text{sele}}\left(E^*_\gamma\right)\sum_{\text{pol}}\left|\frac{\mathcal{A}^{\text{IB}}_{\pm\gamma}}{\mathcal{A}_\pm}\right|^2
\end{aligned}$$

The correction factor with respect to a constant selection efficiency $\varepsilon_{\text{sele}} = \varepsilon_{\text{sele}}(0)$ is then given by the following expression:

$$\Delta = \frac{\hat{G} - \varepsilon_{\text{sele}}(0)G}{\varepsilon_{\text{sele}}(0)G} \tag{14}$$

The expression for the integral $I_\pm(\omega)$ for a constant efficiency has been explicitely given in reference [13], with an accuracy of order ω/M_K, so the calculation has been split in two parts. First, Eq. (14) has been applied with a maximum energy $\omega = 50$ MeV, giving

$$\Delta_{E<50\text{MeV}} = (-1.67 \pm 0.02) \times 10^{-3}.$$

The error has been evaluated by simultaneously changing the two fit parameters by $\pm 1\sigma$ and taking the maximum variation of the acceptance.

Second, the contribution to Δ due to energies above 50 MeV is estimated as follows. The relative contribution to the width from this part of the spectrum has been measured to be $\text{BR}_{\text{rel}} = (2.60 \pm 0.08) \times 10^{-3}$[14]. The error $\Delta_{E>50\text{MeV}}$ has been estimated by comparing the constant efficiency $\varepsilon_{\text{sele}}(0)$ with the average[3)] selection efficiency $\langle\varepsilon_{\text{sele}}\rangle_{E>50\text{MeV}} = (25.1 \pm 0.3)\%$ for this part of the spectrum:

$$\Delta_{E>50\text{MeV}} = \text{BR}_{\text{rel}} \cdot \left(\frac{\langle\varepsilon_{\text{sele}}\rangle_{E>50\text{MeV}} - \varepsilon_{\text{sele}}(0)}{\varepsilon_{\text{sele}}(0)}\right) = (-1.488 \pm 0.002) \times 10^{-3}$$

This contribution is finally summed to the former error, giving a 3×10^{-3} correction factor, which has been applied. It has to be noted that a looser selection, which requires *at least* one track entering the calorimeter (instead of two), would bias the efficiency even less.

The final acceptance, including also the correction due to the tracking efficiency is:

$$\boxed{\varepsilon^\pm_{\text{sele}} = 0.576 \pm 0.001_{\text{stat}} \pm 0.001_{\text{syst}}} \tag{15}$$

10 Trigger and t_0 efficiencies for $K_S \to \pi^+\pi^-$ events

The estimate of the probabilities that, given a selected event, at least a golden-t_0 cluster is found and the event is triggered are discussed in this section. The efficiency for the K_S pions to fix the global-t_0 *has to be estimated directly from data*, for the following reasons:

3) Using a constant average efficiency slightly overestimates the error, since the photon energy spectrum is falling down with E^*_γ.

– not to rely on the simulation of the interactions of low-energy pions in the calorimeter
– because, contrary to the photon clusters of the $K_S \to \pi^0\pi^0$ events, the probability to have a t_0-fixing cluster from one of the two pions, is not so close to 100%.

Both considerations also apply to the trigger efficiency estimate.

10.1 t_0 efficiency

In order to estimate the t_0 efficiency, $\varepsilon_{\mathrm{t0}}$, two different methods have been applied: using the $K_L \to \pi^+\pi^-\pi^0$-tagged data sample, and tuning the Monte Carlo simulation with data-extracted efficiencies.

Exactly as for the $K_S \to \pi^0\pi^0$ sample, direct use has been done of $K_L \to \pi^+\pi^-\pi^0$ events, selected through a t_0-independent algorithm. After having removed any trigger bias, the $K_S \to \pi^+\pi^-$ selection is applied. Clusters close to the impact points of the K_S tracks are assigned to K_S. The t_0 efficiency is finally defined as the fraction of the selected events in which a golden-t_0 cluster is found, among the K_S ones. The results are listed in table 4.

The probability *per single track* coming from the IP and entering the calorimeter to produce a golden-t_0 cluster has been first extracted from various data subsamples, as a function of the track momentum, of the hit region of the calorimeter, of the impact angle and of the particle type (π^+, π^-, μ^+, μ^- are distinguished). These data-extracted probabilities are then used to weight the Monte-Carlo-simulated kinematics of the pair of tracks selected in $K_S \to \pi^+\pi^-$ events; the efficiency of the t_0 condition is calculated as Monte Carlo average of these weight-functions.

Tracks from two different control samples have been used: a K_{crash}-tagged $K_S \to \pi^+\pi^-$ subsample and $\phi \to \pi^+\pi^-\pi^0$ decays. The selection algorithms are similar to those described in Sect. 7 and 4 respectively, with the same conditions on tracks. Both tracks are extrapolated[4)] to the calorimeter surface, and the impact points are calculated. When considering a track, the clusters associated to the other particles in the event are required to be at a distance greater than 100 cm from its impact point. Those clusters are also required to satisfy the golden-t_0 and trigger conditions by themselves. Then, the t_0 efficiencies are calculated in an unbiased way for the clusters produced by the track under study. These are binned as a function of the track momentum and impact angle, separately for barrel or end-cap calorimeters and for particle type (two examples are shown in Fig. 37).

These single-particle efficiencies are plugged into the $K_S \to \pi^+\pi^-$ Monte Carlo simulation and the efficiency $\varepsilon_{\mathrm{t0}}$ for the K_S to satisfy the t_0-cut is calculated. For each Monte Carlo event, a pair of tracks is selected according to the $K_S \to \pi^+\pi^-$ algorithm described above. The t_0 *event*-efficiency is calculated as:

$$\varepsilon_{\mathrm{t0}}\,(\mathrm{event}) = \varepsilon_{\mathrm{t0}}^{\mathrm{track1}} + \varepsilon_{\mathrm{t0}}^{\mathrm{track2}} - \varepsilon_{\mathrm{t0}}^{\mathrm{track1}}\varepsilon_{\mathrm{t0}}^{\mathrm{track2}}$$

where the efficiencies are evaluated in multidimensional bins $\varepsilon_{\mathrm{t0}}^{\mathrm{track}i}\,(p_i \otimes \theta_i \otimes \mathrm{bar/end}_i \otimes \mathrm{type}_i)$. The estimated t_0 efficiency is then obtained averaging over the Monte Carlo events:

$$\varepsilon_{\mathrm{t0}} = \langle \varepsilon_{\mathrm{t0}}\,(\mathrm{event}) \rangle$$

4) With an analytical extrapolation of a helix defined by the track parameters to the calorimeter surface, assuming a costant solenoidal magnetic field [10].

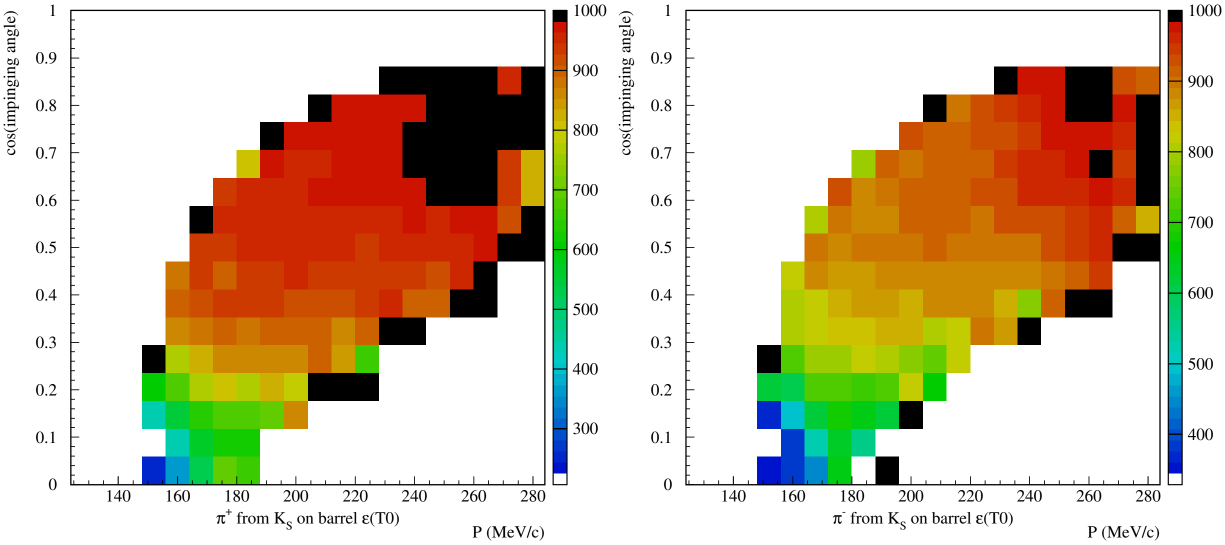

Figure 37: t_0 efficiency as a function of the cosine of the impact angle of the track and of the track momentum, for π^+ (left) and π^- (right) on the barrel calorimeter.

The result is compared with the previous method in Tab. 4. The statistical-systematic error is due to the limited Monte Carlo statistics, the systematic error takes into account the errors on the data-extracted efficiencies.

Method	$\varepsilon^{\pm}_{\mathrm{t0}}$ [%]
$K_L \to \pi^+\pi^-\pi^0$ Summer 2000	$99.4 \pm 0.3_{\mathrm{stat}}$
$K_L \to \pi^+\pi^-\pi^0$ December 2000	$99.0 \pm 0.1_{\mathrm{stat}}$
Single-particle tuned MC	$98.9 \pm 0.1_{\mathrm{sysstat}} \pm 0.1_{\mathrm{syst}}$
Weighted average	99.0 ± 0.1

Table 4: Efficiency that a golden-t_0 cluster is found in events selected as $K_S \to \pi^+\pi^-$. The results obtained by using $K_L \to \pi^+\pi^-\pi^0$ events and by the Monte Carlo simulation, tuned with data extracted efficiencies, are shown. The weighted average is used in the following.

10.2 Trigger efficiency

The trigger efficiency, given the golden-t_0, is estimated similarly as for $K_S \to \pi^0\pi^0$ events. The probabilities for the K_S to fire one or more trigger sectors are combined with the one for the K_L to fire two or more:

$$\varepsilon_{\mathrm{TRG|t0}} = \varepsilon_{\mathrm{L}}\,(\geq 2) + \varepsilon_{\mathrm{L}}\,(1) \times \varepsilon_{\mathrm{S|t0}}\,(1)$$

The time difference with respect to the K_{crash}-cluster is no more sufficient to cleanly separate K_S and K_L clusters, as can be seen in Fig. 38: for low K_{crash} energies, the right tail of the K_S-cluster distribution cannot be clearly disentangled from the left tail of the K_L-fragments one. Despite of this problem, a cut at -2 ns is used to separate K_S and K_L clusters.

The contribution to the trigger sector probabilities of the wrongly assigned sectors can be estimated by changing the K_{crash} energy. The observed K_L sector distribution is

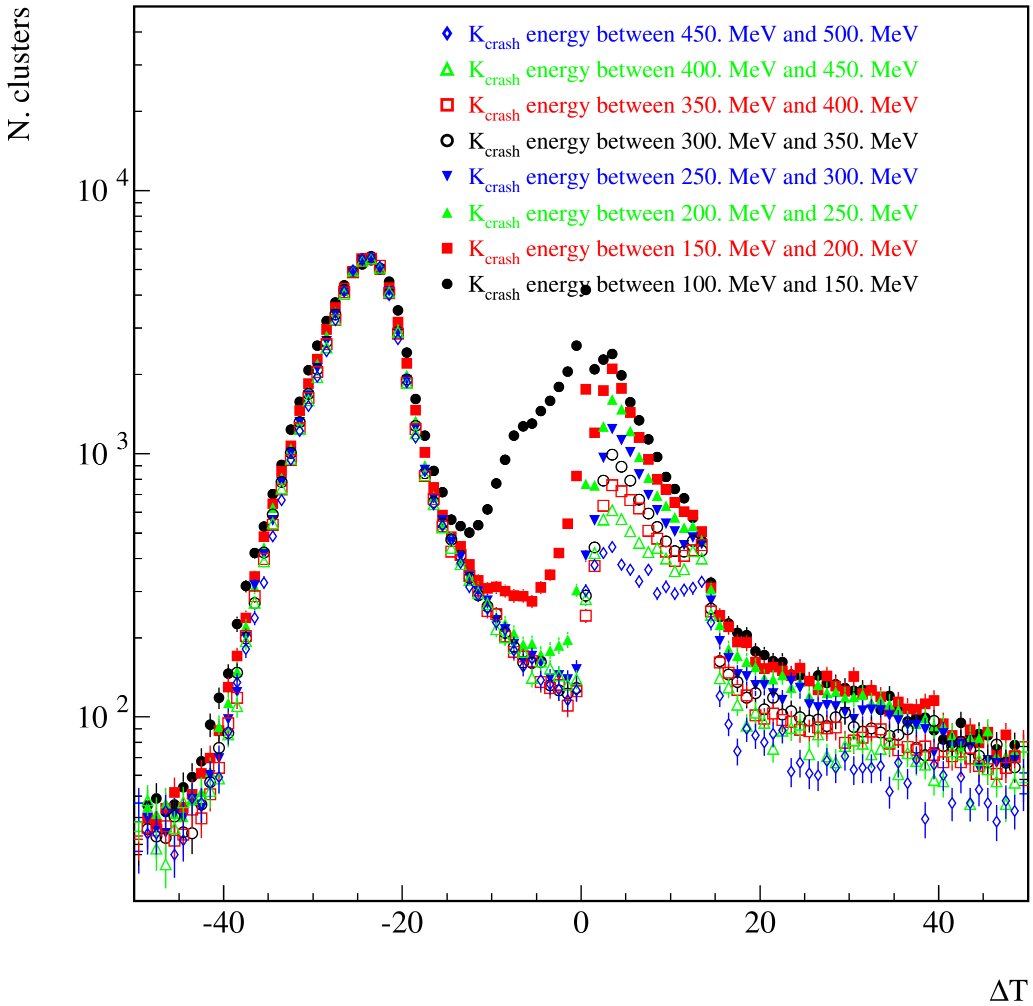

Figure 38: $K_{\rm crash}$-tagged event, identified as $K_S \to \pi^+\pi^-$. Distribution of the difference in time of each cluster with respect to the $K_{\rm crash}$-cluster. In the plot there is one entry for each cluster in the event with energy above 20 MeV ($K_{\rm crash}$-cluster excepted). As the $K_{\rm crash}$ energy increases, the distribution at high times, due to the K_L-cluster-fragments, become more and more depopulated. Nevertheless, the right-tail of the K_S distribution is not cleanly separated from the K_L contribution.

compared with the one obtained in $K_S \to \pi^0\pi^0$ events, where the separation is effective: as shown in Fig. 39, the probability for the $K_{\rm crash}$ to trigger by itself (two or more sectors) in $K_S \to \pi^+\pi^-$ events is lower for $K_{\rm crash}$ energies below 200 MeV. This indicates that a significant fraction of the K_L sectors has been assigned to the K_S.

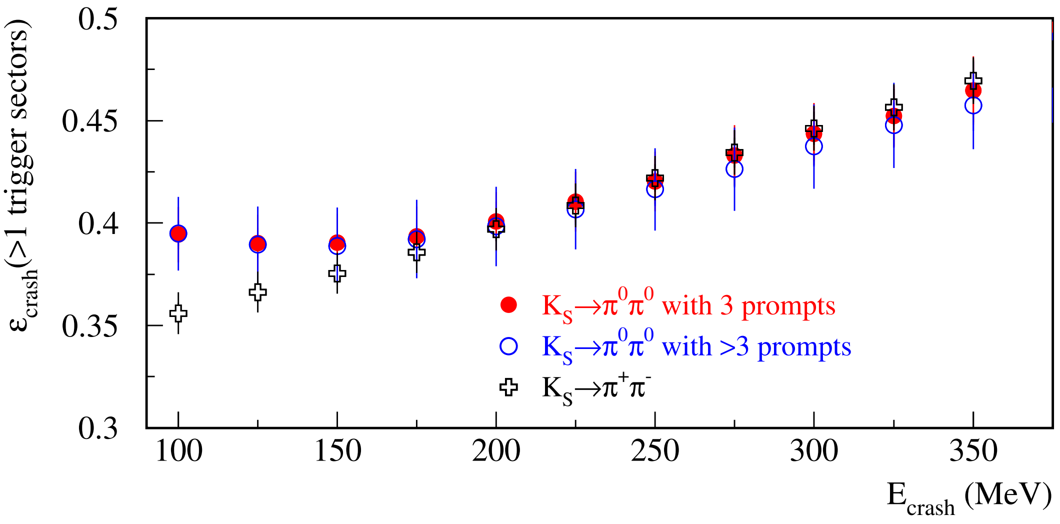

Figure 39: Efficiency for the K_L to satisfy the trigger conditions by itself, in $K_{\rm crash}$ events, as function of the energy cut used in the $K_{\rm crash}$-tagging. The efficiency using $K_S \to \pi^+\pi^-$ sample (crosses) is compared with the one derived by $K_S \to \pi^0\pi^0$ events, selected requiring three (solid circles) or more than four (open circles) prompt clusters.

On the contrary, the probability for the K_S to fire one or more trigger sectors has a smaller absolute variation (Fig. 40): since it is already as high as 98%, it is less sensitive to contributions from misassigned K_L sectors. Hence, the trigger probability, given the t_0, is calculated using this K_S sector-efficiency and the K_L efficiency from $K_S \to \pi^0\pi^0$ events. The result for $K_{\rm crash}$ energy cut at 100 MeV is:

$$\varepsilon_{\rm TRG|t0} = (98.7 \pm 0.1_{\rm syst})\,\%$$

where the systematic error is due to the sectors fired by both the K_S and the K_L and it is estimated as for the $K_S \to \pi^0\pi^0$ (Sect. 5).

Combining with the previous result for the t_0, the overall efficiency is:

$$\boxed{\varepsilon_{\rm t0TRG} = \varepsilon_{\rm t0} \times \varepsilon_{\rm TRG|t0} = (97.6 \pm 0.3)\,\%} \qquad (16)$$

This result is compared with the one obtained using the tuned Monte Carlo; this is also useful to estimate the *single-particle* trigger-sector probabilities of the K_S. These are expressed as a function of the momentum p, and of the coordinate along the fibers. The trigger effective energy thresholds, in fact, depend on the position along the fibers, and of the hit calorimeter region (barrel, end-cap-hot, end-cap-warm, end-cap-cold). Some of these efficiencies are shown in Fig. 41. The sector efficiencies are calculated separately whether the t_0 cut is satisfied ($\varepsilon_{\rm sect|t0}$) or not ($\varepsilon_{\rm sect|\overline{t0}}$). The probability for the K_S to fire one or more trigger sectors and to give the t_0 is then calculated, again as an average over the Monte Carlo events:

$$\varepsilon_{\rm t0sect}\,(\text{event}) = \varepsilon_{\rm t0}\varepsilon_{\rm sect|t0}\,(\text{track 1})\ \text{ OR }\ \varepsilon_{\rm t0}\varepsilon_{\rm sect|t0}\,(\text{track 2}) + \ldots$$

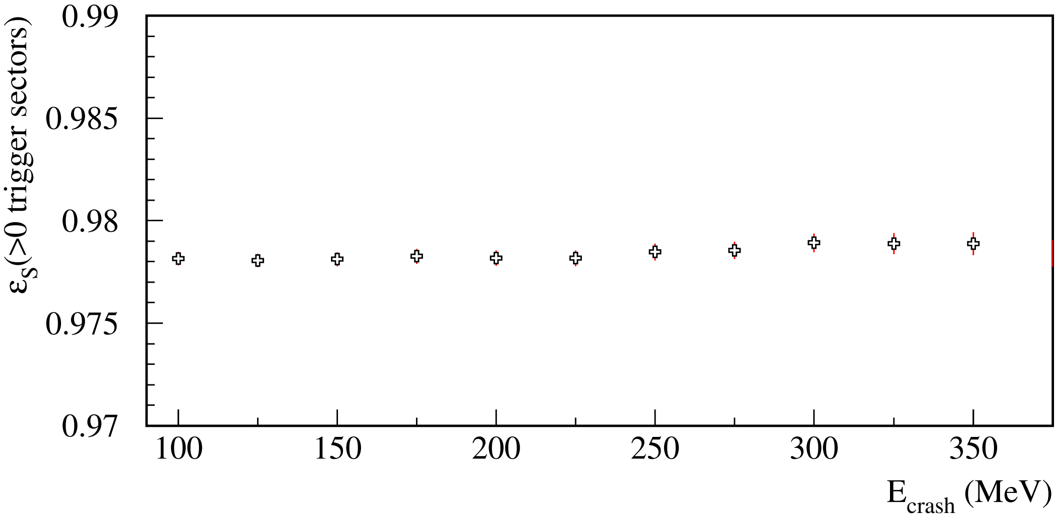

Figure 40: Probability for the K_S to fire one or more trigger sectors, in $K_S \to \pi^+\pi^-$ events. The probability is estimated using events tagged by the $K_{\rm crash}$ algorithm, as a function of the $K_{\rm crash}$ energy cut; the result is stable at the per-mil level.

and, for simplicity, all the other terms, which include the possibility for a track to fire a sector not satisfying the golden-t_0 condition, are not written here. The efficiency for the combined t_0 and trigger conditions is calculated including the trigger sector probability of the K_L:

$$\varepsilon_{\rm t0TRG} = \varepsilon_{\rm L}\,(\geq 2)\,\varepsilon_{\rm t0} + \varepsilon_{\rm L}\,(1) \times \varepsilon_{\rm t0sect}\,(1) = (96.5 \pm 0.3)\,\%$$

The difference with the previous result is due to the contributions to the trigger of the pion fragments and of the accidental clusters, which are not taken into account by this method, which considers only the clusters close to the track-impact point.

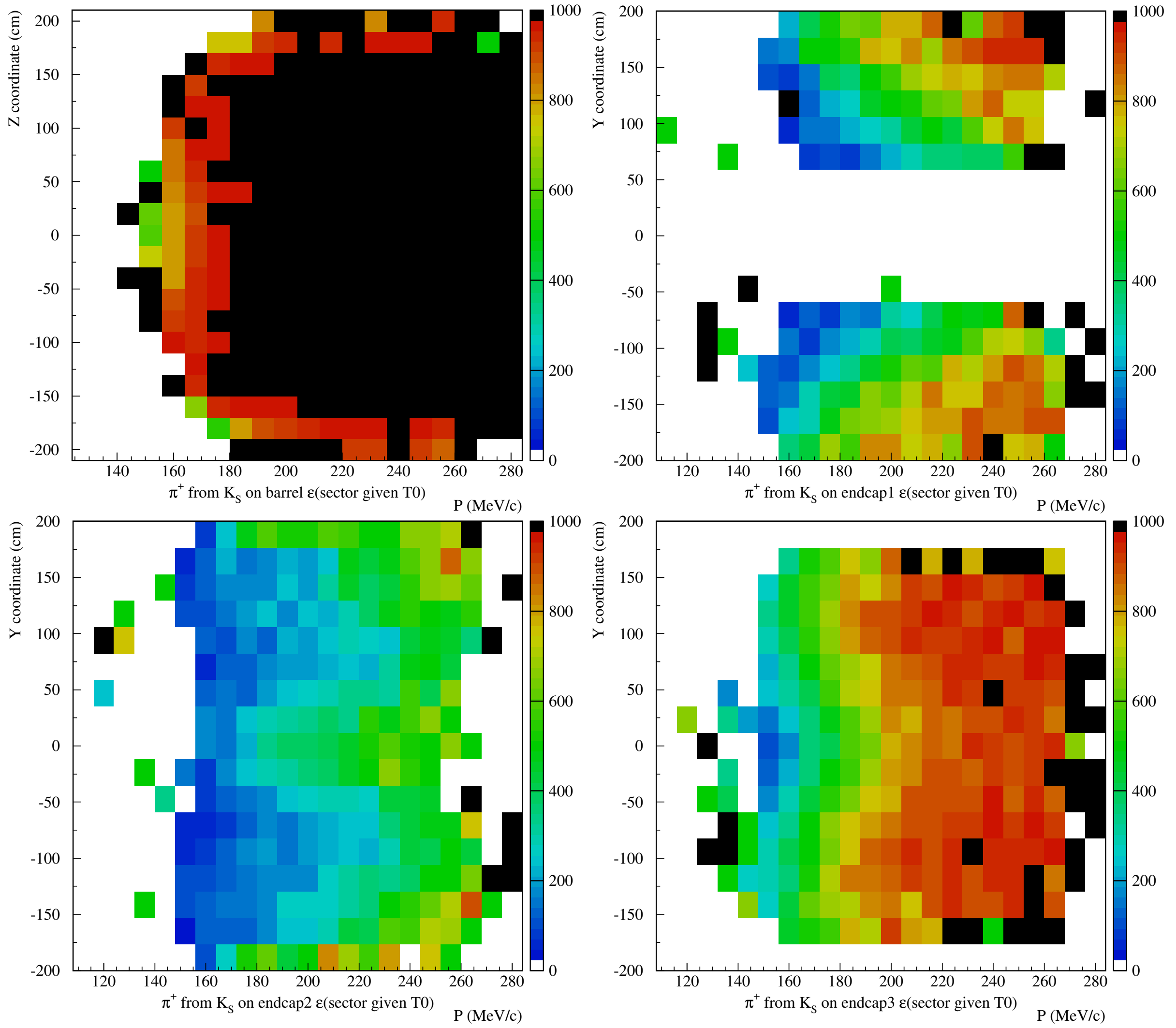

Figure 41: Sector efficiencies for π^+ tracks satisfying the golden-t_0 requirement. Z-coordinate vs momentum on barrel (up left), Y-coordinate vs momentum on end-cap for hot (up right), warm (down left) and cold (down right) trigger sector zones. The different effective-threshold profiles are visible.

11 Cosmic veto corrections for $K_S \to \pi^+\pi^-$ vs $K_S \to \pi^0\pi^0$ events

During the data acquisition, a fast recognition of the cosmic ray events, which occur with a rate of 2.5 KHz, is provided by the trigger: the presence of two fired cosmic-sectors tags a cosmic-ray event [15].

This veto, however, rejects a small fraction ρ_{veto} of $\phi \to K_S K_L$ events, due essentially to the K_{crash} cluster. Assuming an indicative value of 30 mb for the total cross section of the K_L in the calorimeter, the mean free path is of the order of 10 cm. Hence, the overall calorimeter length corresponds roughly to three interaction lengths. It is then possible that a small fraction of the K_{crash} clusters hits the outermost plane, firing one or two cosmic sectors. The correction to the measurement of the ratio of decay widths is the ratio of cosmic-veto "inefficiencies":

$$C_{\text{veto}}^{\pm/00} = \frac{1 - \rho_{\text{veto}}\,(K_S \to \pi^+\pi^-)}{1 - \rho_{\text{veto}}\,(K_S \to \pi^0\pi^0)}$$

This correction is estimated directly from data, since a downscaled sample (2%) of the events otherwise rejected by the veto are instead acquired and reconstructed. The ρ factors are then estimated calculating the fraction x_{veto} of vetoed events among the selected ones, in each K_S channel:

$$\rho_{\text{veto}}\left(K_S \to \pi^+\pi^-, \pi^0\pi^0\right) = 50 \cdot \left.\frac{x_{\text{veto}}}{1 + 49 \cdot x_{\text{veto}}}\right|_{K_S \to \pi^+\pi^-, \pi^0\pi^0}$$

The fractions x_{veto} are $\sim 8 \times 10^{-4}$ for both channels, giving inefficiencies ρ:

$$\rho_{\text{veto}}\left(K_S \to \pi^+\pi^-\right) = (3.7 \pm 0.2_{\text{stat}})\,\%$$

$$\rho_{\text{veto}}\left(K_S \to \pi^0\pi^0\right) = (3.9 \pm 0.2_{\text{stat}})\,\%$$

The fractional difference of the values is around 5%, confirming the dominant contribution of the K_L interactions in the loss. The correction factor is finally:

$$\boxed{C_{\text{veto}}^{\pm/00} = 1.002 \pm 0.003_{\text{stat}}} \tag{17}$$

The results refer to ~ 6 pb^{-1} of integrated luminosity, during the October-November 2000 data taking; a 100-MeV cut on the K_{crash} energy has been used. The statistical error on the C_{veto}-correction is a non negligible contribution to the total error.

12 Results

In this section the results of the analysis are summarized. In order to check its stability, the measurement of the ratio $\Gamma(K_S \to \pi^+\pi^-)/\Gamma(K_S \to \pi^0\pi^0)$ has been performed dividing the whole Year 2000 statistics in four different subsamples. The observed number of selected events and their ratio are listed in Tab. 5.

The ratio $R_{\text{corr}} = T^{\pm}/T^{00}$ of decay amplitudes is obtained from the raw ratio $R_{\text{obs}} = N^{\pm}/N^{00}$, by applying all the efficiency corrections:

$$\frac{N^{\pm}}{N^{00}} = \frac{T^{\pm}}{T^{00}} \cdot \frac{\varepsilon_{\text{crash}}(E_{\text{cut}})}{\varepsilon_{\text{crash}}(E_{\text{cut}})} \cdot \frac{\varepsilon_{\text{sele}}^{\pm}}{\varepsilon_{\text{sele}}^{00}} \cdot \frac{\varepsilon_{\text{t0trg}}^{\pm}}{\varepsilon_{\text{t0trg}}^{00}} \cdot R_{\text{tag}}^{\pm/00} \cdot C_{\text{veto}}^{\pm/00}$$

where:

Year 2000 period	Int. Lum. [pb^{-1}]	$N^{\pm}$	N^{00}	$R_{\rm obs}$
Summer	3.53 pb^{-1}	259 586	197 389	$1.315 \pm 0.004_{\rm stat}$
Oct.-Nov.	6.15 pb^{-1}	549 664	407 635	$1.348 \pm 0.003_{\rm stat}$
Nov.	3.90 pb^{-1}	358 312	266 453	$1.345 \pm 0.003_{\rm stat}$
Nov.-Dec.	3.92 pb^{-1}	359 243	265 476	$1.353 \pm 0.003_{\rm stat}$

Table 5: Summary of the results for the observed number of events in four subsamples of the Year 2000 data taking. The numbers refer to a $K_{\rm crash}$ energy cut of 100 MeV.

- the efficiency $\varepsilon_{\rm crash}$ for the K_L to produce a $K_{\rm crash}$ cluster with energy greater than $E_{\rm CL}$ exactly cancels out in the ratio;
- the selection efficiencies $\varepsilon^{\pm,00}_{\rm sele}$ have been calculated given the $K_{\rm crash}$-tag, Eq. (6) and Eq. (15) respectively;
- the t_0 and trigger (given t_0) efficiencies $\varepsilon^{\pm,00}_{\rm t0trg}$ for the selected events are calculated, Eq. (8) and Eq. (16) respectively;
- the ratio of tag efficiencies $R^{\pm/00}_{\rm tag}$ has been calculated using a subsample of selected (and triggered) $K_S \to \pi^+\pi^-$ events (Sect. 2.3);
- the cosmic-veto correction $C^{\pm/00}_{\rm veto}$ has been calculated using the selected downscaled events, Eq. (17).

As already explained in Sect. 2.3, in order to lower the systematic error on the $R_{\rm tag}$ correction, the $E_{\rm cut}$ value can be optimized. While in the Summer sample actually the systematic error is stable also for a 100 MeV cut, in all of the other samples this decreases significantly with the $K_{\rm crash}$ energy (see Fig. 16). Therefore all the applied corrections except for the acceptance have to be evaluated as a function of the $K_{\rm crash}$ energy.

The $R_{\rm tag}$ correction is shown as a function of the $K_{\rm crash}$ energy in Fig. 15. The t_0 and trigger efficiencies, the cosmic veto corrections have been then evaluated separately for each sample as a function of the $E_{\rm cut}$ value. The results are shown in Fig. 42. The

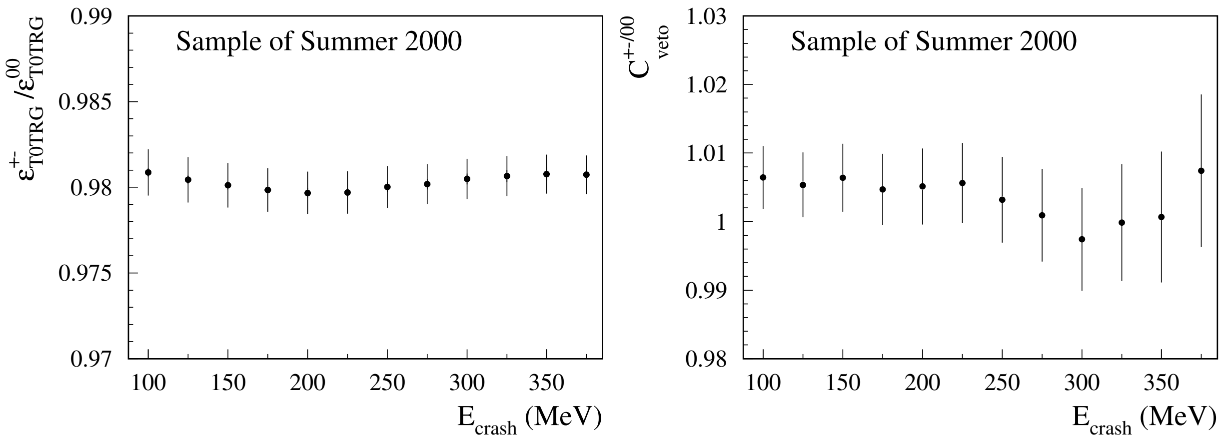

Figure 42: Ratio of t_0 and trigger efficiencies (left) and cosmic veto correction (right) as a function of the $K_{\rm crash}$ energy cut, for the Summer 2000 period of data taking.

ratio of the number of observed events is shown in Fig. 43, as a function of the $K_{\rm crash}$ energy cut. The ratio of decay amplitudes obtained correcting for all selection efficiencies is shown in Fig. 44: the total error is dominated by the systematic contribution.

The systematic error is, in turn, the quadrature sum of the statistical-systematic

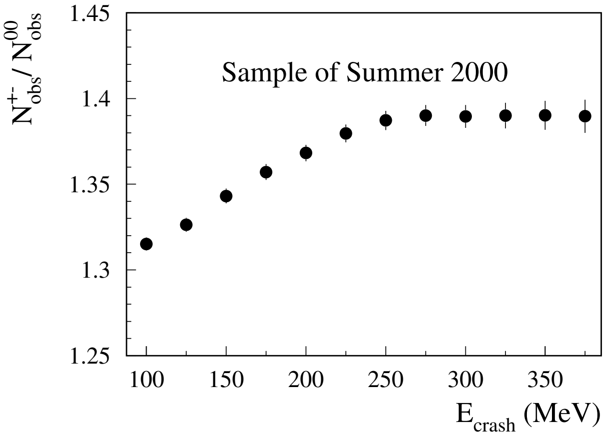

Figure 43: Ratio of the selected number of events, before applying all the efficiency corrections, as a function of the $K_{\rm crash}$ energy cut for the Summer 2000 period of data taking.

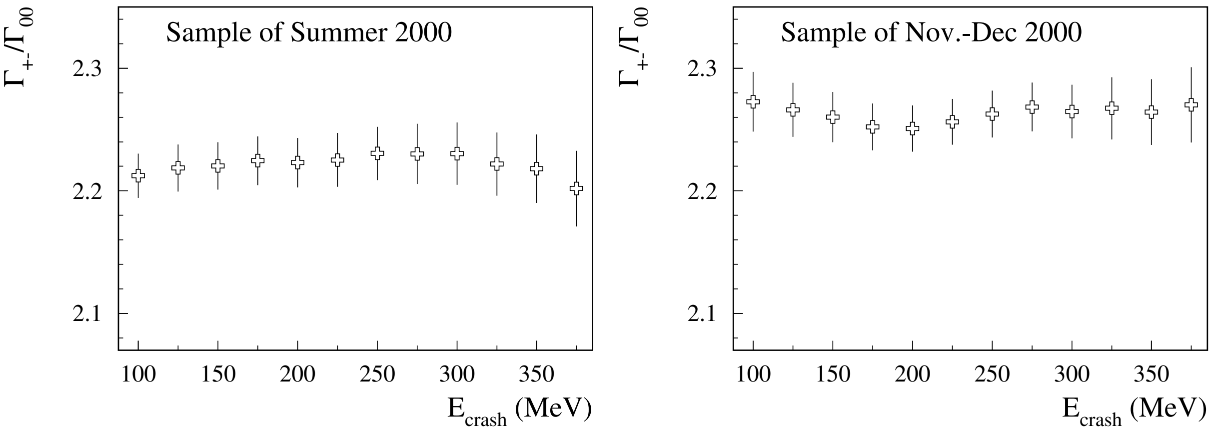

Figure 44: Ratio of the number of events, after all efficiency corrections have been applied, as a function of the $K_{\rm crash}$ energy cut, for the Summer (left) and December (right) 2000 period of data taking.

and pure systematic contributions: the former is due to the Monte Carlo statistics or to the data statistics used to estimate the efficiencies, while the latter measures the uncertainty proper of the method used. These errors are shown in Fig. 45. The statistical-systematic error has two main contributions: the cosmic-veto correction (the factor 50 used in the downscale), which dominates the total error at high energies, and the uncertainty in the TCA contribution to the tag bias, which is independent on the $K_{\rm crash}$ energy. The pure systematic error is dominated by the uncertainty in the β^* window acceptance, which increases at low energies (the difference in the tails of the β^* distributions), while at higher energies the errors on $\varepsilon^{00}_{\rm sele}$ (prompt cluster counting) and $\varepsilon^{+-}_{\rm sele}$ (tracking efficiency) become also relevant.

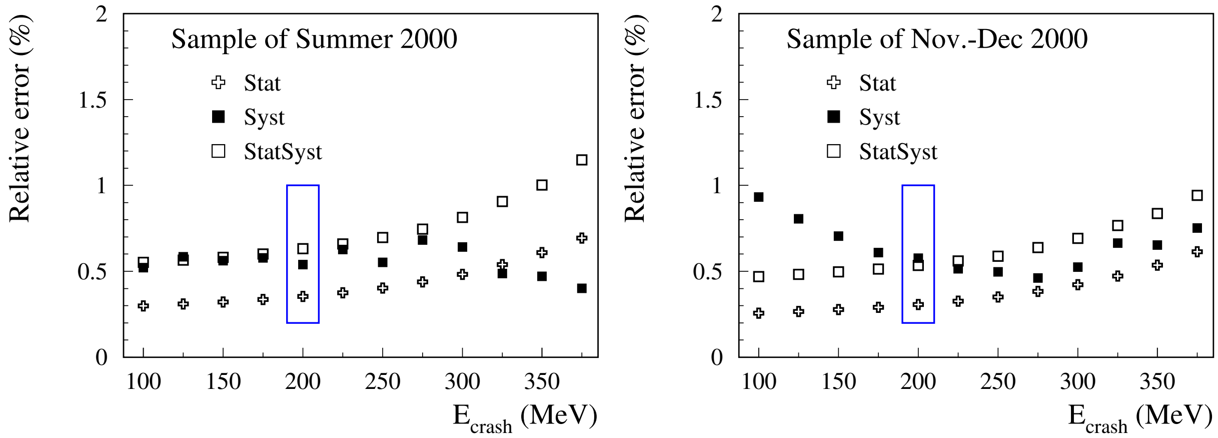

Figure 45: Relative errors as a function of the $K_{\rm crash}$ energy, for the Summer 2000 (left) and December 2000 (right) periods. The chosen cut is also shown (dashed box).

The cut chosen in order to minimize the total error is $E_{\rm cut} = 200$ **MeV.** The measurements on the four samples are listed in Tab. 6. The relative spread of the measurements on the four samples, is of 7×10^{-3}, corresponding to a chi-square of $\chi^2_0 = 5.17$ for 3 degrees of freedom ($P(\chi^2 > \chi^2_0) = 16\%$). The final measurement of the ratio is

Period of Y2000	$\Gamma(K_S \to \pi^+\pi^-)/\Gamma(K_S \to \pi^0\pi^0)$			
Summer	2.220	$\pm 0.008_{\rm stat}$	$\pm 0.012_{\rm syst}$	$\pm 0.015_{\rm syststat}$
Oct.-Nov	2.235	$\pm 0.006_{\rm stat}$	$\pm 0.011_{\rm syst}$	$\pm 0.011_{\rm syststat}$
Nov.	2.246	$\pm 0.007_{\rm stat}$	$\pm 0.010_{\rm syst}$	$\pm 0.012_{\rm syststat}$
Dec.	2.241	$\pm 0.007_{\rm stat}$	$\pm 0.013_{\rm syst}$	$\pm 0.012_{\rm syststat}$

Table 6: Summary of the results in four subsamples of the Year 2000 data taking, obtained by applying a $K_{\rm crash}$ energy cut of 200 MeV.

obtained as a weighted average:

$$\boxed{\Gamma(K_S \to \pi^+\pi^-)/\Gamma(K_S \to \pi^0\pi^0) = 2.236 \pm 0.003_{\rm stat} \pm 0.015_{\rm syst}} \tag{18a}$$

$$\boxed{\Gamma(K_S \to \pi^+\pi^-)/\Gamma(K_S \to \pi^0\pi^0) = 2.236 \cdot (1 \pm 0.001_{\rm stat} \pm 0.007_{\rm syst})} \tag{18b}$$

The weights used are the statistical errors. Since the cosmic veto correction is stable over the periods, and the error on its estimate is purely statistical, this correction has been averaged. The associated error has been included in the total systematics. The different contibutions to the final systematic error are disentangled in Tab. 7.

Source	Relative error [10^{-3}]-units
Tag bias	5.5
Tracking	2.6
Cluster counting	2.0
Trigger	1.0
Cosmic veto	2.1

Table 7: Relative contributions to the final systematic error.

13 Conclusions

A measurement of $\Gamma(K_S \to \pi^+\pi^-)/\Gamma(K_S \to \pi^0\pi^0)$ has been presented, based on the statistics of 17 pb^{-1} integrated by KLOE during the Year 2000. The event yield allowed to reach a relative statistical error of 1×10^{-3}, thus imposing a stringent control of the possible systematics. This has been achieved by estimating the various efficiency corrections mainly from data subsamples (except for geometrical acceptances), not to rely on the Monte Carlo simulation of low energy pion and kaon interactions in the calorimeter. In particular, the corrections relevant for the analysis are: trigger, tracking, and prompt cluster counting efficiencies; the ratio of tagging efficiencies; the inefficiency induced by the cosmic veto (applied at the trigger level). Presently the systematic error is limited by the accuracy in the control of the tagging efficiency.

A looser β^* cut has been already introduced in the online event reconstruction for the Year 2001 data sample. This provides a simple way to reduce the bias in the tagging, by an offline adjustment of the β^* cut. In order to achieve a systematic control at the level of 10^{-3}, a dedicated study of the Monte Carlo effective energy threshold is also needed to address the photon detection efficiency to the cited accuracy.

Altough the present measurement has been shown to be fully inclusive of all radiated photons, it is planned to repeat it as a function of the photon energy.

14 Acknowledgments

We are very grateful to G. Cabibbo, who has set up this analysis and who has started a big part of the studies discussed here; our work follows the route he has traced.

We want to warmly acknowledge F. Bossi, who coordinated this work, for the illuminating discussions, and for the enormous effort of *n-tuple* production.

We also want to thank S. Miscetti, who helped us in gaining a deeper understanding of the clustering, and provided us precious suggestions.

Finally we are grateful to C. Gatti, for the studies on the calorimeter time scale correction, and for many useful discussions on different items, such as the $K_{\rm crash}$ energy cut, the cosmic veto correction, and the $K_S \to \pi^+\pi^-(\gamma)$ acceptance.

References

[1] G. Cabibbo, Ph.D. thesis, Università di Roma "La Sapienza", (2000).

[2] F. Ambrosino *et al.*, KLOE **memo 177** (1999).
A. Antonelli *et al.*, KLOE **memo 194** (1999).

[3] M. Adinolfi *et al.*, **LNF-01/017 (P)** (2001)
C. Bini *et al.*, KLOE **memo 205** (2000).

[4] G. Pirozzi *et al.*, KLOE **memo 225** (2000).

[5] G. Cabibbo, T. Spadaro, KLOE **memo 210** (2000).

[6] S. Di Falco, KLOE **memo 173** (1998).
[7] G. Pirozzi *et al.*, KLOE **memo 220** (2000).
[8] A. Menicucci, G. Finocchiaro, KLOE **memo 203** (1999).
A. Menicucci, G. Finocchiaro, KLOE **memo 204** (1999).
[9] C. Bini *et al.*, KLOE **memo 207** (2000).
[10] T. Spadaro, Ph.D. thesis, Università di Roma "La Sapienza", XIV Ciclo.
[11] T. Spadaro *et al.*, KLOE **memo** in preparation.
[12] F. Bossi *et al.*, KLOE **memo 223** (2000).
[13] V. Cirigliano, J. F. Donoghue, and E. Golowich, Eur. Phys. J. **C18**, 83 (2000).
[14] E. J. Ramberg *et al.*, Phys. Rev. Lett. **70**, 2525 (1993).
[15] M. Palutan, Ph.D. thesis, Università di Roma "Tor Vergata" (2000).